Carbon gels derived from phenolic-oil for pollutants removal in water phase

S. Schaefer, P. Gadonneix, A. Celzard, Vanessa Fierro

Carbon gels derived from phenolic-oil for pollutants removal in water phase

S. Schaefer, P. Gadonneix, A. Celzard, V. Fierro*

Université de Lorraine, CNRS, IJL, F-88000 Epinal, France

* Corresponding author : Vanessa Fierro: vanessa.fierro@univ-lorraine.fr

Abstract

The gelation of a low value-added industrial waste, phenolic oil (PO), was successfully carried out for the first time in the presence of an acid catalyst and paraformaldehyde (PF), which is a by-product of the formaldehyde industry. Therefore, the use of PO and PF can be considered a win-win situation and as an attempt to valorise these 'wastes' and integrate them into a circular economy. A broad range of formulations has been explored, and the optimal preparation conditions in terms of materials' homogeneity and yield have been identified for gels dried in different ways, leading to xerogels, cryogels and aerogels, as well as to their carbonaceous counterparts after pyrolysis at 900°C. The porous textures of the latter materials were studied in depth, and the results allowed selecting one carbon xerogel for adsorption studies of a reference molecule, methylene blue (MB), in the aqueous phase. Kinetic and equilibrium measurements, as well as the calculation of associated thermodynamic parameters, allowed elucidating the detailed adsorption mechanisms of MB in this type of carbon gel.

Keywords: Carbon gels; Water remediation; Phenolic-oil; Adsorption thermodynamics; Methylene blue

38

1. Introduction

Pekala et al. were the first to propose the synthesis of gels based on resorcinol and formaldehyde [1-3]. The principle of gel synthesis is similar to that of resins, but uses a much higher dilution of the reactive mixture. Among the different types of phenolic resins, resoles and novolacs are the most known and synthesised [4].

The polycondensation of such organic precursors and the crosslinking of the resultant oligomers give, in the case of gels, nodular structures having high surface area and porosity. So far, most of the first gels were based on resorcinol or phenol, with formaldehyde as the crosslinking agent [5-7]. In this case, the gelation step is usually carried out in a closed vessel under heating (e.g. at 85°C). Before closing the system, a catalyst is added to the mix of precursor and crosslinker. The catalyst can be either acidic or basic (NaOH, Na_2CO_3 and HCl are most commonly used) [8]. After a period varying from a few hours to several days, the heating is stopped and the system is open. The materials thus obtained are called hydrogels because their porosity is saturated by an aqueous phase. After drying, the organic gels can be pyrolysed to obtain carbonaceous materials, whose resultant surface area typically ranges from 500 to 800 $m^2 g^{-1}$, and can reach even more than 2000 $m^2 g^{-1}$ after activation [9-11].

Due to the toxicity and high cost of the usual precursors, many researches focused on "greener" precursors and crosslinkers. Many new "green" precursors such as tannins or lignin were also used, in combination or not with classical precursors (e.g. phenol or resorcinol), in order to obtain gels [12-18]. Regarding the crosslinker, formaldehyde can be replaced by furfural, which can also be biosourced [19-21]. Another approach would be to use waste from the chemical industry to produce high added-value materials such as porous carbon gels.

Coal tar is obtained as a by-product of coal carbonisation and it is submitted to different processes for its conversion into valuable chemicals or light fuels [22-26]. Coal tar distillation

leads to different fractions, phenolic oil (PO) among them. To the best of our knowledge, there are only two studies dealing with gels and carbon gels based on PO in the open literature [27, 28]. A low-value PO from the company Bilbaína de Alquitranes – SA (BASA, Spain), mainly containing phenol, coumarone, o,m,p-xylene, indane, indene, o,m,p-cresol, and naphthalene, has been used in this work as carbon gel precursor. Looking at the reactivity of these different components for the synthesis of gels, one can say that the use of phenol for such application has already been well explored, and consistent results were reported [5, 19, 21, 29, 30]. Several authors have also synthesised gels using cresol as precursor [31-36]. As for indene, it can react with phenol in acidic conditions to give indanylphenol. Some patents reported that indanylphenol can be used to obtain resins and thus can polymerise in acidic conditions and under heating (70-140°C) [37, 38]. Coumarone can also react with indene to form coumarone-indene resins [39, 40]. In addition, coumarone has also been used in the past to produce phenol-modified coumarone-indene resins [41, 42]. Naphthalene can also be found in phenolic oil and is known to react with epichlorohydrin to form epoxy that can eventually polymerise to epoxy resins [43, 44]. If naphthalene is alkoxylated and submitted to special conditions (multistep process, concentrated acid), it can condensate with formaldehyde [45]. The reaction of part of the naphthalene in the PO used in this work is thus not excluded, although its intrinsic reactivity is probably lower than that of the other chemical species mentioned above.

Thus, PO should be sufficiently reactive and hence worth testing for synthesising gels. The main difficulties are the different reactivities of the various chemicals contained in the phenolic oil as well as their initial dilution state in less or even non-reactive species (indane, xylene…). Another challenge in synthesising gels based on phenolic oil is the hydrophobic nature of the latter, which prevents proper mixing with formaldehyde, generally in the form of a 37 wt. % of solution in water, stabilised by 10% of methanol. Therefore, a solvent other than

water should be used. Thus, many studies have proposed the use of alcohols as solvents (e.g. n-propanol, propan-1-ol or isopropanol) [7, 32, 46]. In addition, the catalyst should also have good solubility with the solvent and be preferentially organic.

Once porous materials are successfully prepared, some applications should be considered. Among them, water remediation is relevant and remains a hot topic. The removal of pollutants from aqueous wastewater is indeed a problem of paramount importance, whether in the event of an accidental spill or for the permanent removal of chemicals that are not eliminated using conventional water treatment technologies. The removal of these chemical species can be achieved using nanoporous materials such as activated carbons [47], zeolites [48], silica-based materials or even organic materials such as organic gels [49] or biomass materials [50-52]. Water pollutants can be inorganic, such as ions of heavy metals [53-55], or organic, such as antibiotics [56, 57] or other pharmaceutical components [58]. Despite the diversity of pollutant/sorbent systems presented in current research works, methylene blue (MB) remains a reference molecule in the case of preliminary studies of liquid phase adsorption of ionic and organic pollutants [59-61]. Even if many studies presented the characteristics of the MB adsorption on carbonaceous materials, only a few reported the use of carbon gels for that purpose [62, 63]. In addition, the thermodynamic models used to calculate enthalpy and entropy of adsorption are, according to some authors, often misused [64]. The origin of such errors in estimating thermodynamics parameters is due to the non-rigorous evaluation of the equilibrium constant [64].

In this study, we successfully prepared carbon gels from PO, and their application for the removal of pollutants from an aqueous phase was tested by adsorption of MB. In addition, we compared different approaches to calculate the thermodynamic adsorption parameters and we were able to elucidate the detailed adsorption mechanisms of MB in this type of carbon gel. Enthalpy and entropy of adsorption were calculated over the full range of concentration and

equilibrium coverage and using two different methodologies: the isosteric method and the Van't Hoff equation.

2. Experimental

2.1. Preparation of organic gels

The composition of the phenolic oil (PO), provided by Bilbaína de Alquitranes, S.A. (BASA, Spain), used this work for preparing carbon gels, is given in Table S1 (Supplementary material). This PO mainly contains phenol, coumarone, indene, m-p-cresols and o-cresol at the following, respective weight fractions: 14.80, 2.34, 11.54, 7.38 and 3.64 %. Coumarone, indene and phenol can form resins under specific conditions [39, 41, 42]. In addition, in presence of Lewis acids (e.g. $FeCl_3$, $AlCl_3$) and alkyl halides (e.g. dichloroethane, trichoromethane), indene can also undergo Friedel-Crafts reaction and form hypercrosslinked networks [65, 66]. For these reasons, their respective contents are taken into account in the reactive fraction. Thus, the reactive fraction in the PO is *a priori* expected to be approximatively 40 wt. %, because naphthalene has not be taken into account (indane is also assumed not to react under the chosen synthesis conditions). The rest of the PO components are considered solvents.

The catalyst chosen and found suitable for our system was para-toluenesulphonic acid, PTSA (Merck®, synthesis grade, 98 %). This is mainly due to its high solubility in organic solvents and its strong acidic character. Indeed, unlike inorganic salts (i.e., NaOH or Na_2CO_3) or aqueous solutions containing acidic catalyst (i.e., HCl or HNO_3), PTSA is highly soluble in organic solvents. In addition, PTSA is commonly used as catalyst for crosslinking reactions to produce novolac resins based on hydrophobic precursors such as cardanol [67]. Similar resins were also successfully converted into porous carbon materials [68]. Paraformaldehyde, PF (Merck®, synthesis grade, 95 %), which is soluble in isopropanol (Carlo Erba, spectroscopy grade, 99.8%), was used as crosslinker.

For describing the preparation of an organic gel, Job et al. suggested the use of the following molar ratios: resin-forming (possibly phenolic) monomers to catalyst (P/C), resin-forming (possibly phenolic) monomers to crosslinker (P/F), and dilution ratio (D = total number of moles of solvent to number of moles of reagent) [8, 69, 70]. The P/C and P/F ratios were fixed at about 15 and 0.55, respectively, while D was taken in the range 0.5-1.8. The ratios were calculated taken into account phenol, coumarone, indene, m-p-cresols and o-cresol as resin-forming monomers. The P/C and P/F ratios were fixed in order to evaluate only the effect of the dilution on the textural properties of the gels. A representation of these ratios can be found in Figure S1 (red dashed lines), and Table 1 shows the formulations tested. Figure S1a shows the decrease of the reagent content (PF: total mass of reagents (resin-forming monomers and paraformaldehyde) to total mass of resin) while the S1d shows the linear increase of D.

The general preparation protocol is now described: isopropyl alcohol (IPA) was first vigorously stirred with PO during 2 min in a 50 mL beaker. Then, PTSA was added and dissolved in the blend by vigorous stirring for 2 to 5 minutes. Finally, paraformaldehyde was added and the mixture was vigorously stirred once more. At room temperature and in such a proportion, the solubilisation of paraformaldehyde is very difficult to achieve. Thus, the stirring was stopped when a large fraction was already dissolved and when the other fraction was well dispersed (no agglomerates) in the solution (5-10 min stirring). During the whole mixing step, the beaker was covered with an aluminium foil in order to minimise the evaporation of the solvent and other volatile species (the temperature of the room was also kept at 15°C for this purpose). Then, the mixtures were poured into test tubes (at 90% filling) that were hermetically sealed afterwards, and put in a ventilated oven at 85°C. After 30 min, the tubes were shaken vigorously by hand to dissolve completely the paraformaldehyde. Then the samples were left to gel at 85°C for 5 days. The gel formed after 2-3 days, but curing

continued for 5 days to obtain well polymerised and crosslinked material. After hardening, the sample tubes were broken; the gels were cut into centimetre-sized cylinders and washed under stirring with absolute ethanol (Carlo Erba®, 99.9%) for 5 days (orbital shaker, 90 rpm, 30°C). The ethanol was renewed every day. Note that, because no water was used in the preparation process, the resultant materials cannot be called hydrogels but are solvogels instead.

Table 1: Composition of the formulations tested.

Formulation name	Isopropyl alcohol (g)	Para-formaldehyde (g)	PTSA (g)	PO (g)	Isopropanol fraction (wt. %)
5 g	5	3.123	0.64	15	21.04
7.5 g	7.5	3.123	0.64	15	28.56
10 g	10	3.123	0.64	15	34.77
12.5 g	12.5	3.123	0.64	15	39.98
15 g	15	3.123	0.64	15	44.43
17.5 g	17.5	3.123	0.64	15	48.26
20 g	20	3.123	0.64	15	51.60

2.2. Drying and pyrolysis of organic gels

Convective drying, leading to xerogels, was carried out in an oven for 2 days at 85°C. Since conventional drying may induce the collapse of the pores due to capillary forces exerted at the interface between the solid and the liquid being evaporated, the resultant materials may be less porous than desired, and therefore not reach high specific surface areas.

Two other drying methods were thus investigated to minimise the collapse of the pores. Cryodesiccation or freeze-drying, leading to cryogels, avoids the formation of the liquid menisci but form ice crystals instead. If water is present, these crystals may increase the pore size and therefore produce materials with a rather coarse porous texture. Moreover, cracks can appear in the cryogel and form “megalopores” (millimetre-sized pores). Prior to the cryodessication, the ethanol was thus exchanged with either ultrapure water or *tert*-butanol (tBu) (Acros Organics®, 99.5 %, extra pure) for 3 days. The advantage of tBu is to avoid the formation of large ice crystals in the material while the advantage of using water is its low

cost. The cryodesiccation was carried out in a HETO PowerDry PL6000 freeze-dryer. First, the materials, impregnated with water or tBu, were frozen at – 90°C for 24 h and evacuated at 10 Pa for 3 days.

The last drying method involves a supercritical fluid and leads to aerogels, and supercritical CO_2 (critical point 31°C, 7.3 MPa) is the most used for this application. First, the ethanol was exchanged with liquid CO_2, which was then heated up to 40°C in order to reach supercritical conditions. After this step, the pressure was slowly (0.04 MPa min^{-1}) decreased to pass from the supercritical state to the gaseous state. In this way, no liquid/gas interface appears and drying can be theoretically achieved without causing collapse and damage to the pore structure. Thus, this method is supposed to preserve the textural properties of the gels. The process was carried out in an Autosamdri-815 Tousimis® critical point drier. The exchange of ethanol with liquid CO_2 was carried out 4 times before raising the temperature to 40 °C. Additional details about the supercritical drying procedure can be found elsewhere [71] [13].

After drying, the materials were pyrolysed in a tubular furnace, using a quartz tube (diameter 25 mm) continuously flushed with nitrogen (100 STP cm^{-3} min^{-1}). The heating rate was set at 2°C min^{-1} up to the final temperature of 900°C, which was held for 2h. The latter temperature was selected in order to ensure a high final carbon content [12-14, 27] and a developed texture, which can be analysed by DFT models that were indeed developed for materials containing quasi-exclusively carbon [72, 73]. The carbon gels were named by a letter (A for aerogel, C for cryogel, X for xerogel), followed by the mass of phenolic oil as indicated in the formulations detailed in Table 1. For instance, X_12.5 is the carbon xerogel obtained by convective drying of the organic xerogel called OX_12.5 in the following, derived from the formulation 12.5 g (itself named from the initial amount of IPA that had been used), and submitted to carbonisation at 900°C.

2.3. Characterisation

2.3.1. Weight and volumes changes

During pyrolysis, a partial gasification of the materials takes place, and they therefore lose weight. The carbon yield Y_{pyr} of the pyrolysis is expressed as:

$$Y_{pyr} = \frac{m_{final\ carbon}}{m_{initial\ gel}} \times 100 \quad (1)$$

where *m* are masses measured before and after pyrolysis.

During drying, the material can shrink both due to pore collapse and desorption of the liquid from inside the solid matrix (un-swelling effect). During pyrolysis, gases leave the solid matrix and the network shrinks further. In both cases (drying and pyrolysis), the radial shrinkage of the samples is quantified by:

$$RS_{step} = \frac{Ø_{initial} - Ø_{final}}{Ø_{initial}} \times 100 \quad (2)$$

where RS_{step} represents the radial shrinkage for a synthesis step (drying or pyrolysis) and Ø stands for the diameter of the sample (initial or final).

2.3.2 Ultimate analyses

Ultimate analyses of samples for the determination of their elemental composition were carried out with a CHONS elemental analyser (Vario El Cube, Elementar) as reported elsewhere [74].

2.3.3 Electron microscopy observations

Scanning electron microscopy was used for the determination of samples' morphology, using a FEI QUANTA600FEG microscope and a secondary electrons detector. Additional information about the model of the methodology can be found elsewhere [75].

2.3.4 Gas adsorption

An automatic adsorption device (ASAP 2020, Micromeritics) was used for the textural characterisation of carbon gels. The samples were degassed under vacuum at 150°C until the pressure stabilised at about 0.2-0.4 mPa for more than 48 h. Further degassing was carried out at the measuring port for at least 6 h. The cold and warm volumes were determined after nitrogen or carbon dioxide adsorption to avoid helium entrapment in the narrowest pores. The analyses were carried out by nitrogen and carbon dioxide adsorption at – 196°C and 0°C, respectively. All the data were treated using the Microactive® software from Micromeritics.

The surface area calculated by the Brunauer-Emmett-Teller (BET) method, A_{BET}, was obtained using the BET equation in the appropriate range of relative pressures [76]. A_{BET} was only determined to compare our results with those reported in the literature, and not used here for other calculations because of the corresponding well-known underestimation or overestimation of surface area by the BET equation when dealing with microporous or mesoporous materials, respectively. The micropore volumes were obtained using the Dubinin-Radushkevich ($V_{\mu\text{-}DR}$) equation, and were also given for comparison with the literature [77, 78]. The pore size distributions (PSDs) were obtained using the non-local density functional theory (NLDFT) from the Solution of Adsorption Integral Equation Using Splines (SAIEUS®) routine. SAIEUS® has the advantage of combining both CO_2 and N_2 adsorption data to obtain more accurate PSDs [79, 80]. The smoothing parameter λ was set constant and equal to 4 for all the samples in order to allow the comparison between different PSDs. This value is the most common and the lowest defined by the SAIEUS® routine for our set of samples. The average micropore ($L_{0\text{-}NLDFT}$), mesopore (L_{meso}) and total pore (L_{tot}) sizes using NLDFT and volume (dV) weighting were calculated using the PSD. The NLDFT method was also used to determine the surface area S_{NLDFT} by integrating the PSDs over the whole range of pore sizes. The Barrett, Joyner and Halenda method (BJH) was also used to calculate the

mesoporous volumes from the desorption branch of the isotherms [81]. The BJH results were refined by using the Kruk-Jaroniec and Sayari optimisation method [82, 83].

Finally, a comparison of the different models was made: (i) total pore volumes, according to Gurvich ($V_{P/P0=0.98}$) and NLDFT; (ii) surface areas, from the BET method and the NLDFT; (iii) micropore volumes, from the DR method and the NLDFT; (iv) mesopore volumes, from NLDFT and the difference between $V_{P/P°=0.98}$ and the micropore volume from the NLDFT.

2.3.5. Potentiometric titration

The potentiometric titration for the determination of the surface chemistry was applied only to the carbon gel having the most developed textural properties and synthesised with the cheapest procedure. It consisted in the titration of an acidic solution (pH = 3) of 25 mL in which 1 g of carbonaceous material was dispersed. Before this initial pH adjustment with 0.1 mol L^{-1} HCl, the solution was degassed during several hours using argon bubbling in order to remove the solubilised CO_2. The titration was carried out using sodium hydroxide (NaOH, 0.1 mol L^{-1}) as titration agent. In order to obtain a high number of titration data (200 points), an automatic titration system (Titrando 905, Metrohm) was used. Each point corresponds to the pH value of the solution after adding 0.01 mL of NaOH solution. The titration curve gave access to the proton-binding isotherm, which can be analysed either by using its first derivative, or by using a deconvolution model giving access to the pK_a distribution of the material [84].

2.4. Methylene blue adsorption

2.4.1. Kinetics studies

Kinetic studies of MB adsorption consisted in measuring the MB uptake by the X_12.5 carbon gel up to 25 h, using a thermostatic bath (25°C) under stirring. For that purpose, an accurately weighted amount (W) of 12.5_X carbon gel (5-10 mg), previously dried (24 h, 105°C) ,was introduced into conical flasks containing 50 mL of an aqueous solution of MB (bi-distilled water, pH ≈ 5.8). The adsorption experiments were performed by considering two different initial MB concentrations (c_0) of 10 and 90 mg L^{-1}.

The temporal evolution of the concentration of MB in the solution was measured during 25 h, using a UV-Vis spectrophotometer (Lambda 35, Perkin Elmer) at a wavelength of 554 nm, corresponding to the maximum absorbance of MB. This optimal wavelength was previously evaluated by measuring the absorption spectrum of an aqueous solution of MB at 10 mg L^{-1}. The absorbance data were then converted into concentration using a calibration plot, built for the MB concentration range from 0 to 10 mg L^{-1}.

During the whole adsorption process, the conical flasks were totally covered by aluminium foil to avoid MB photo-degradation under UV light. After adsorption, appropriate dilutions of MB solutions were performed for respecting the linearity of Beer-Lambert's law. The absence of pH drift during the experiment was checked by measuring the pH with a glass electrode before and after the adsorption process. The adsorbed amounts at time t and at equilibrium, q_t and q_e, respectively, were calculated as follows:

$$q_t = \frac{(c_i - c_t)\,V}{W} \quad (3)$$

$$q_e = \frac{(c_i - c_e)\,V}{W} \quad (4)$$

where c_i, c_t and c_e are the initial concentration, the concentration at a given time t, and the concentrations at equilibrium, respectively. V is the volume of the MB solution, and W is the dry weight of carbon gel.

The modelling of the adsorption kinetics was carried out using the pseudo-first (equation (5)) and pseudo-second (equation (6)) order models [85]:

$$\log(q_e - q_t) = \log(q_e) - \frac{k_1\, t}{\ln(10)} \quad (5)$$

$$\frac{t}{q_t} = \frac{1}{k_2\, {q_e}^2} + \frac{t}{q_e} \quad (6)$$

where k_1 and k_2 are the rate constants of the pseudo-first or pseudo-second order kinetic models, respectively.

The quality of the fit was assessed by the determination coefficient (R^2) and the chi-square (χ^2) value of the associated linear plots. In addition, the classical intra-particle diffusion model was also applied [86]. The corresponding equation reads:

$$q_t = K_{id}\, t^{0.5} + R_i \quad (7)$$

where K_{id} is the intra-particle diffusion constant and R_i is the diffusion resistance [86].

2.4.2. Equilibrium adsorption studies

The equilibrium points were obtained using 10 mL of MB solution with concentrations of 10 to 180 mg L^{-1} while the amounts of carbon were in the range of 0.3 to 0.6 g L^{-1}. The equilibration time was set at five days, at least. The adsorption experiments were carried out at three different temperatures (15°C, 25°C and 45°C) and a constant pH (5.8-6). The glass vials containing the suspensions of carbon gel in MB aqueous solution were kept hermetically sealed and protected from light during the whole adsorption process.

Three different adsorption models were selected: Freundlich, Langmuir and Sips. The Freundlich (equation (8)) and the Langmuir (equation (9)) adsorption models read as follows:

$$n_{ads} = N_F\ (c_e)^b \quad (8)$$

$$n_{ads} = N_L\ \frac{K_L\, c_e}{1 + K_L\, c_e} \quad (9)$$

where n_{ads} is the adsorbed amount at equilibrium, and N_F, b, N_L and K_L are constants. N_L represents the maximum adsorption capacity and K_L is the Langmuirian equilibrium constant.

The Sips model, also called Langmuir-Freundlich model, is defined as follows:

$$n_{ads} = N_S\ \frac{K_S\ (c_e)^{1/n}}{1 + K_S\ (c_e)^{1/n}} \quad (10)$$

where N_S, $1/n$, and K_S are constants. The isotherms were directly fitted using the Levenberg-Marquardt algorithm implemented in the Matlab® software. The relevance of a specific model was evaluated by observing the values of determination coefficient (R^2) and Chi-square (χ^2) of the fits.

2.4.3. Thermodynamic studies

The free energy of adsorption is defined by the following equation:

$$\Delta G_{ads} = -RT \ln (K) \quad (11)$$

where K is the equilibrium constant while R and T are the universal gas constant and the absolute temperature, respectively. Sometimes the equilibrium constant is defined using a distribution constant (equations (12) and (13)). In this case, the distribution constant is defined as the ratio of the adsorbed amount (q_e, in mg g^{-1}) to the equilibrium concentration (c_e, in mg L^{-1}). Another definition of the distribution constant uses the adsorbed amount (c_{ads}, in mg L^{-1}) (equation (13)). Some authors suggest that the most rigorous method consists in using c_{ads}

instead of q_e [64]. Consequently, the definition of the distribution constant given by equation (13) is the only one used here for further investigation.

$$K = \frac{q_e}{c_e} \quad (12)$$

$$K = \frac{c_{ads}}{c_e} \quad (13)$$

The free energy of adsorption is also equal to:

$$\Delta G_{ads} = \Delta H_{ads} - T\,\Delta S_{ads} \quad (14)$$

Thus, plotting ΔG_{ads} as a function of temperature gives access to the enthalpy through the intercept (H_{ads}) of the linear regression, and the entropy of adsorption through the slope (ΔS_{ads}).

These results were compared to those obtained using the isosteric method, based on the assumption of thermodynamic equilibrium:

$$\Delta G_{ads} = 0 \quad (15)$$

This condition guarantees the validity of the Clausius-Clapeyron equation. Once derived, ΔH_{ads} is obtained [74, 87]:

$$\Delta H_{ads} = -R\left(\frac{\partial \ln(c_e)}{\partial\, T^{-1}}\right) \quad (16)$$

The isosteric heat is defined by:

$$q_{st} = -\Delta H_{ads} \quad (17)$$

The isosteric heat of adsorption was obtained by plotting the quantity $\ln(c_e)$ as a function of $1/T$. The equilibrium condition also gives access to the isosteric entropy of adsorption:

$$\Delta S_{ads} = \frac{\Delta H_{ads}}{T} \quad (18)$$

Such an assumption is only valid at equilibrium and is the expression of the well-known entropy-enthalpy compensation principle [88]. As the range of temperature is likely to be considered small (i.e., 15 – 45°C), the adsorption temperature will be considered to be equal to the average of the three temperatures used for the adsorption isotherms. The isosteric heat and the entropy of adsorption were both estimated, after assessment of the quality of the fit, using the most relevant adsorption model presented above (Langmuir, Freundlich or Sips).

Some authors report ΔH_{ads} as the enthalpy of displacement. Indeed, it refers both to desorption of solvent molecules (i.e., water) from the adsorbent surface and to adsorption of the solute (i.e., MB) [89]. In this case, the thermodynamic quantities result from both a dilution effect (the solvent being desorbed from the sorbent surface) and an adsorption effect (the solute being desolvated and adsorbed on the sorbent surface). Johnson et al. used similar terminology to present an equation similar to that used for the isosteric method [90]:

$$\Delta_{dpl}h_{st} = -\frac{RT^2}{\phi_1^1}\left(\frac{\partial \ln\left(a_2^1\right)}{\partial T}\right)_{x_2^a} \quad (19)$$

where $\Delta_{dpl}h_{st}$ is the displacement enthalpy of compound 1 (solvent) by compound 2 (solute) obtained using the isosteric method, ϕ_1^1 is the volume fraction of compound 1 in the bulk phase and a_2^1 is the activity of the compound 2 in the bulk phase at constant molar fraction x_2^a of solute in the adsorbed phase. In the assumption of "infinite dilution", such equation can be reorganised and reduced to the following equation, which is similar to equation (16) [91].

$$\Delta_{dpl}h_{st} = -RT^2\left(\frac{\partial \ln\left(C_e\right)}{\partial T}\right)_{q_e} \quad (20)$$

Thus, the isosteric method must have the characteristic of a displacement enthalpy. Therefore, the thermodynamic parameters calculated here are only apparent. Such apparent thermodynamic parameters are supposed to include both adsorption of solute and desorption of solvent. Thus, the terms displacement or adsorption will be interchangeably used here.

3. Results and discussion

3.1. Main characteristics of solvogels and carbon gels

3.1.1. Colour and homogeneity of solvogels

The gel synthesis method is summarised in Figure 1. The gels had a colour going from dark brown to almost white (Figure 1b), depending on the amount of solvent. Below 5 to 7.5 g of isopropanol (21-29 wt. % of the formulation), demixing occurred during gelation, leading to two different phases in the formulation 5 g (see Figures S2 and 1b). Above 15 g of IPA, the obtained material was also heterogeneous. The concentrations of the precursors of the resin indeed became too low to reach the gel point. As a result, the gel was heterogeneous with some parts resembling agglomerated flakes (see formulations 15 g and 17.5 g in Figures S2 and 1b). Between 7.5 and 15 g of isopropanol (≈ 29-44 wt. %), the gels had a homogeneous

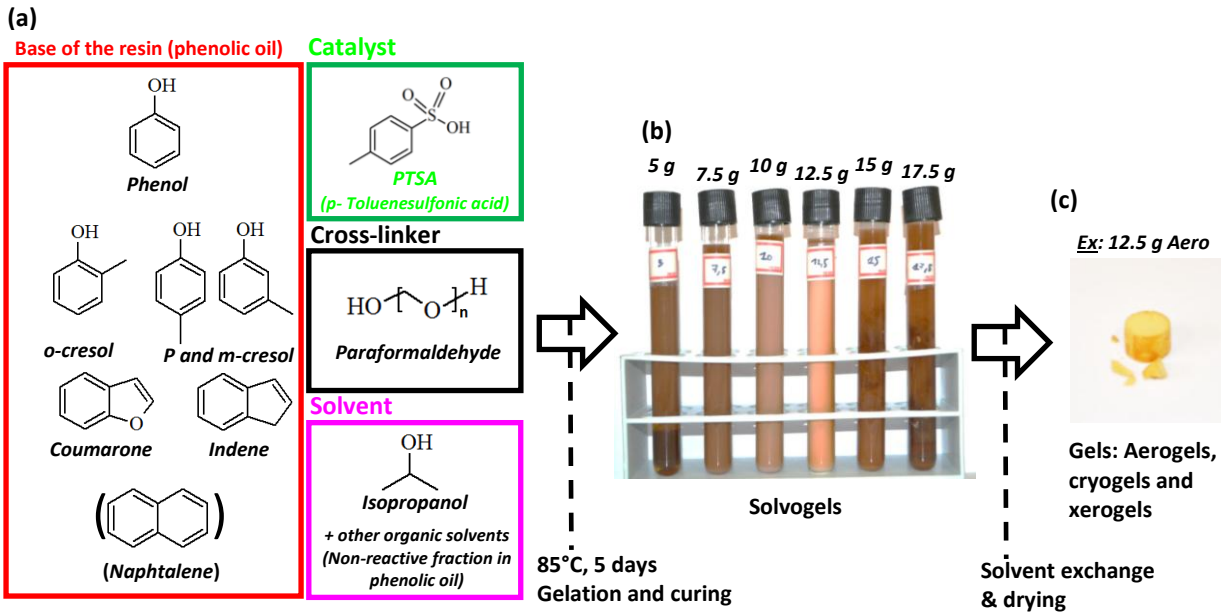

appearance and a light brown to orange colour.

Figure 1. Scheme of the gel synthesis: (a) main compounds of phenolic oil; (b) photograph of the solvogels in their tests tubes, and (c) photograph of the 12.5 g organic aerogel.

After drying, the aerogels retained colours and homogeneity similar to their wet counterparts. Due to the formation of ice crystals and stresses induced by capillary forces, the cryogels and xerogels suffered shrinkage and cracks, respectively. After pyrolysis, the gels were black and had the usual glassy appearance of conventional carbon gels of phenolic origin.

3.1.2. Yield and shrinkage

The shrinkage of the gels during drying is due to both the collapse of the pores and the evaporation of the solvent. Figure 2a shows the shrinkage of the different solvogels during drying. As expected, the shrinkage was higher for convective drying (xerogels) than for cryodesiccation (cryogels) and supercritical drying (aerogels). However, when using more than 12.5 g of isopropanol, the shrinkage was similar for all gels, which could be explained by the higher rigidity of the partly phase-separated (flake-like) structure obtained (see again Figure S2). The shrinkage of the gels during the supercritical drying was slightly higher than during cryodesiccation with water as solvent, about 7.5 %.

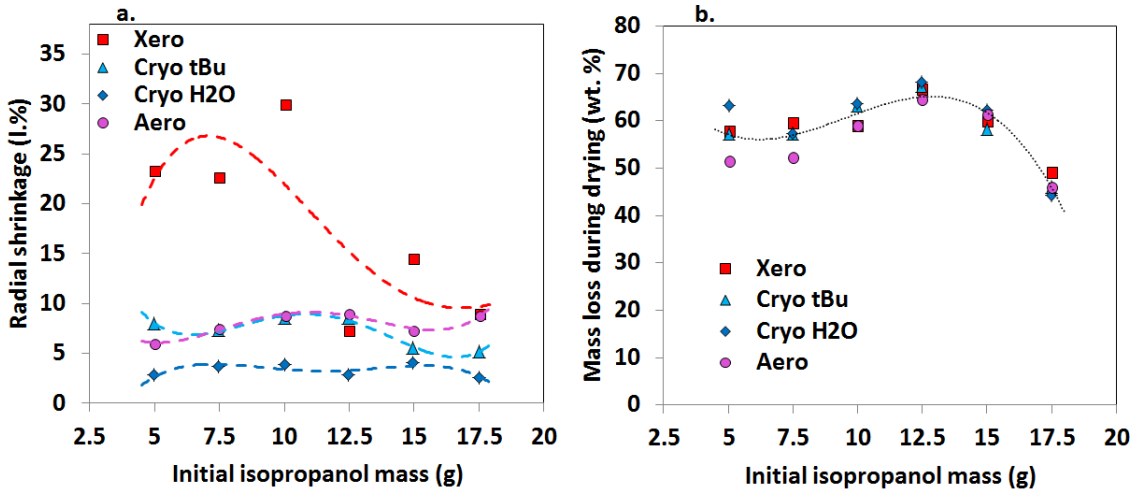

Figure 2. (a) Radial shrinkage, and (b) weight loss during drying of organic gels, depending on the amount of isopropyl alcohol in the formulation.

The shrinkage that occurs during the cryodesiccation depended on the solvent (Figure 2a). The use of water instead of tBu decreased the shrinkage by almost 5%. This can be explained

by the size of the water ice crystals, which are the largest and burst the material structure, and which somewhat compensates the shrinkage occurring during drying due to solvent desorption. For cryodesiccation, the shrinkages of the two sets of materials (Cryo_tBu and Cryo_H_2O in Figure 2a) were similar when using more than 15 g of isopropanol in the formulation, probably due to the higher rigidity of the separated phase, as mentioned above.

The weight loss during drying gives information on the porosity. Despite the different solvents used in the different drying methods, the weight losses were remarkably similar and independent of the drying mode (Figure 2b). The weight loss increased from 50 to 65 % when the amount of isopropanol increased from 5 to 12.5 g. As the shrinkage varied a little in this range for aerogels and cryogels, it can be concluded that the porosity increased in this range of isopropanol amounts. Above 12.5 g of isopropanol in the formulation, the weight loss decreased. However, this indicates that, due to phase separation and at least for cryogels and aerogels, the porosity decreased when the amount of solvent increased too much. At this point, an assumption can already be made: the materials synthesised with an amount of isopropanol close to 12.5 g should have the most developed porous texture due to their combined highest weight loss and lowest shrinkage.

Figure 3 shows both the carbon yield and the radial shrinkage when the organic aerogels have been subjected to pyrolysis. A minimum carbon yield was obtained when using 12.5 g of isopropanol while the shrinkage showed opposite behaviour. Maximum shrinkage was obtained when using 10 g of isopropanol.

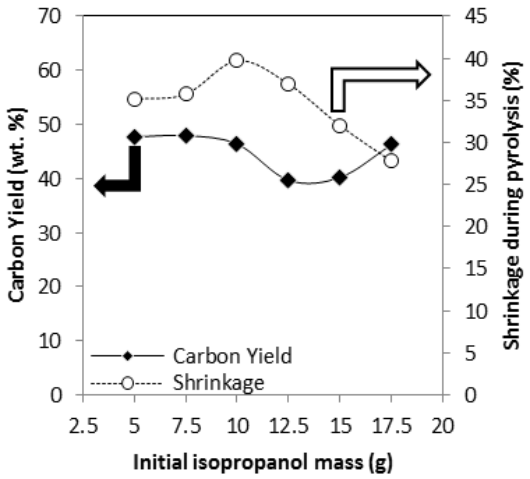

Figure 3. Carbon yield (Y_{carb}) and shrinkage during pyrolysis.

3.1.3. Elemental composition

The elemental composition of one the carbon aerogels, as well as that of two cryogels and one xerogel based on the formulation using 12.5 g of IPA are presented in Table 2. Concerning the latter formulation, the composition of one organic xerogel is also given.

Table 2: Elemental composition the gels and of the 12.5 g organic xerogel.

	H (wt.%)	**C (wt.%)**	**N (wt.%)**	**O (wt.%)**	**S (wt.%)**
OX_12.5 (organic xerogel)	6.2	78.4	0.6	13.6	1.1
After carbonisation					
A_7.5	0.7	95.5	0.7	3.1	0.0
A_10	0.7	95.0	0.8	3.4	0.0
A_12.5	0.6	95.0	0.5	4.0	0.0
A_15	0.6	94.5	0.8	4.1	0.0
A_17.5	0.7	94.3	0.8	4.2	0.0
C_H_2O_12.5	0.6	94.7	0.5	4.2	0.0
C_tBu_12.5	0.5	95.5	0.5	3.5	0.0
X_12.5	0.6	94.7	0.5	4.3	0.0

The organic xerogel OX_12.5 already contains a high percentage of carbon (78.4 wt. %), comparable to that of the PO. Indeed, if we consider only phenol, o-m-p cresols and

coumarone as reactive species in the PO, the elemental composition of the reactive fraction would be C: 77.45 wt. %, H: 6.68 wt. %, and O: 15.87 wt. %. These percentages are thus very similar to those of the organic xerogel OX_12.5 presented in Table 2. However, the percentage of carbon in OX_12.5 is slightly higher than the last calculated, suggesting that a small fraction of indene could still react. In addition, the presence of sulphur suggests that the catalyst (PTSA) could partly be reacted with, or at least, be trapped in, the solid matrix.

The carbon content in all the other gels, around 95 wt. %, indicates that the materials obtained after pyrolysis really deserve being named "carbons".

3.1.4. Samples' morphology

SEM images (Figure 4a) revealed the expected nodular structure, very typical of phenolic gels, with nodule sizes far below the micrometre. After digital filtering, binarisation and application of a particle detection routine (ImageJ software), the size distribution of nodules could be obtained (Figure 4b). While large carbon aggregates (up to 500 nm) can be noticed, the smallest ones have an average Feret diameter close to 150 nm.

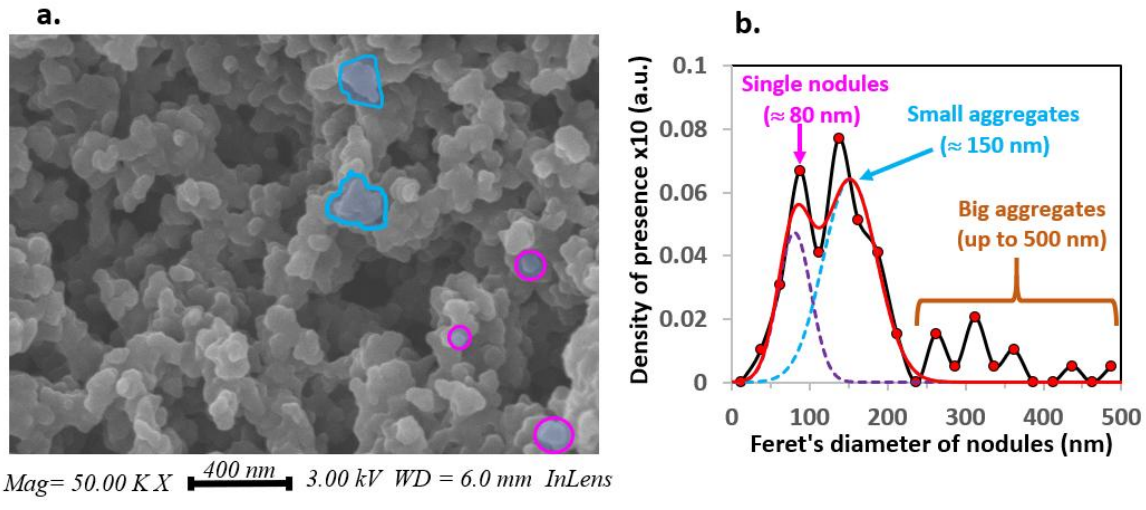

Figure 4. (a) SEM imaging of the X_12.5 carbon xerogel, and (b) size distribution of its carbon nodules.

The smallest observable structures are the individual carbon nodules. Their average Feret diameter is close to 80 nm and is similar to what is observed in other carbon gels derived from resorcinol-formaldehyde [92] or tannins-formaldehyde resins [13].

3.1.5. Textural properties

Figure 5a shows the nitrogen adsorption-desorption isotherms (at – 196°C) made on carbon aerogels. The final adsorbed amount, at P/P_0 = 0.98, increased from 18 to 187 cm^3 STP g^{-1} when the amount of isopropanol increased from 7.5 to 12.5 g, and decreased to 44 cm^3 STP g^{-1} when 17.5 g of isopropanol have been used.

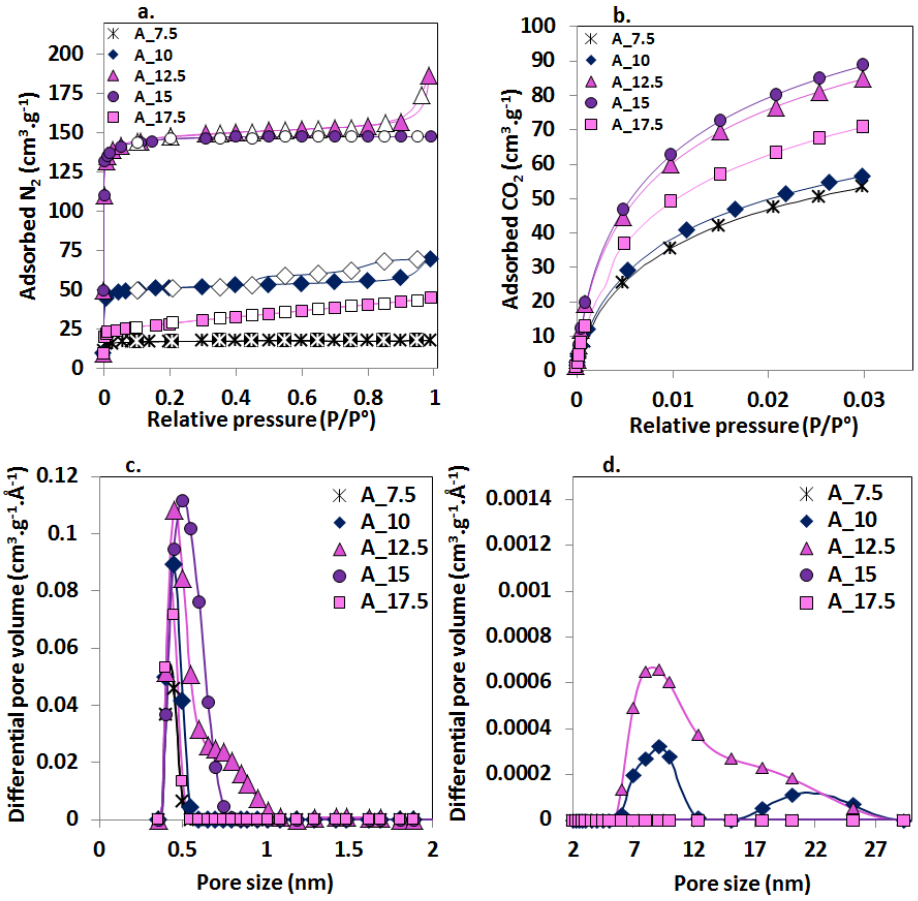

Figure 5. (a) Nitrogen and (b) carbon dioxide adsorption isotherms of carbon aerogels, and corresponding (c) micropore and (d) mesopore size distributions calculated by NLDFT.

The N_2 adsorption isotherms of A_7.5 and A_15 carbon aerogels are pure type Ia [93], with a narrow knee at low pressure and a perfectly horizontal plateau, which is characteristic

of microporous solids. The isotherm of A_17.5 is a combination of types Ia and II [93] and shows a sharp knee and a non-horizontal plateau, which is characteristic of solids with a narrow microporosity and mesoporosity. The isotherms of A_10 and A_12.5 are of mixed types Ia and IV [93]. Indeed, they both exhibit a sharp knee and a hysteresis at relatively high relative pressures, indicating the development of wide mesopores. Carbon dioxide adsorption isotherms (Figure 5b) give access to the amount of ultramicropores and so thus show that the ultramicroporous volume increased when the amount of isopropanol in the formulation increased to 15g. Higher amounts of isopropanol resulted in a reduction in the ultramicroporous volume.

Table 3 shows the BET area (A_{BET}) of the carbon aerogels. An optimum of A_{BET} is located between formulations 12.5 and 15 g, with similar areas 593 and 594 $m^2 g^{-1}$, respectively. This observation of an optimum is consistent with the previous analysis of the isotherms (Figures 5a and 5b).

Figure 5c presents the micropore size distributions of the carbon aerogels obtained using the NLDFT model applied to both nitrogen and carbon dioxide adsorption isotherms. The texture is in good agreement with the basic analysis of the isotherms, predominantly microporous for most materials. In the microporous range, the pore size distributions (PSDs) are unimodal with a single peak in the pore size range of 0.4-0.6 nm, which changes only slightly with the amount of solvent in the formulation. However, the PSDs became broader when the amount of isopropanol increased from 7.5 to 12.5 g and narrower again above 12.5 g of isopropanol. Only the carbon aerogels derived from the 10 g and 12.5 g formulations had a slightly mesoporous texture with some peaks between 6 and 30 nm but with a very low amplitude (Figure 5d). These very low amplitudes confirm the predominantly microporous nature of the carbon gel texture.

Table 3 shows that A_{BET} is much lower (68-649 $m^2\ g^{-1}$) than S_{NLDFT} (192-948 $m^2\ g^{-1}$) due to the limitations of the BET method together with the limitations of nitrogen diffusion at –196°C. Thus, the combined use of CO_2 and N_2 adsorption isotherms in the NLDFT model allows a more accurate description of the texture, and is more likely to take into account the smallest pores. The total pore volumes obtained according to the Gurvich method (V_{tot_98}) and those obtained using the 2D-NLDFT-HS (V_{tot}) were similar, but the DR method, applied only to N_2 adsorption, leads to an underestimation of the microporous volume (0.03-0.25 $cm^3\ g^{-1}$) compared to the NLDFT method (0.04-0.25 $cm^3\ g^{-1}$) that takes also into account the fraction of micropore volume only accessible to CO_2. Logically this underestimation of the microporous volume by the DR method leads to an overestimation of the mesoporous volume (calculated as $V_{meso} = V_{tot\_98} - V_{\mu\_DR}$) compared to that obtained using the NLDFT (V_{meso}). Therefore, the average micropore size L_0 obtained using the NLDFT model was considered the most reliable.

Table 3. Textural parameters of the carbon gels calculated by different methods.

	Textural parameters (classical / **NLDFT**)				
Materials	A_{BET} / $\boldsymbol{S_{NLDFT}}$ ($m^2\ g^{-1}$)	V_{tot_98} / $\boldsymbol{V_{tot\_NLDFT}}$ ($cm^3\ g^{-1}$)	V_{μ_DR} / $\boldsymbol{V_{\mu\_NLDFT}}$ ($cm^3\ g^{-1}$)	V_{meso} / $\boldsymbol{V_{meso\_NLDFT}}$ ($cm^3\ g^{-1}$)	L_{0_DR} / $\boldsymbol{L_0}$ **(dV)** (nm)
A_7.5	68 / **192**	0.04 / **0.04**	0.03 / **0.04**	0.01 / **0.00**	0.52 / **0.44**
A_10	200 / **401**	0.11 / **0.11**	0.08 / **0.09**	0.03 / **0.02**	0.50 / **0.46**
A_12.5	593 / **860**	0.29 / **0.29**	0.23 / **0.23**	0.06 / **0.06**	0.47 / **0.59**
A 15	595 / **921**	0.24 / **0.24**	0.23 / **0.24**	0.01 / **0.00**	0.46 / **0.54**
A_17.5	102 / **299**	0.07 / **0.07**	0.04 / **0.07**	0.03 / **0.00**	0.47 / **0.44**
C_tBu_12.5	649 / **948**	0.32 / **0.32**	0.25 / **0.25**	0.07 / **0.07**	0.48 / **0.58**
C_H_2O_12.5	629 / **908**	0.31 / **0.31**	0.24 / **0.24**	0.07 / **0.07**	0.48 / **0.60**
X_12.5	620 / **891**	0.34 / **0.34**	0.25 / **0.24**	0.09 / **0.10**	0.89 / **0.62**

The PSDs of the materials in the mesopore range were also estimated by applying the BJH method with the KJS correction to the data of the nitrogen desorption branches of the isotherms (Figure S3). Due to the inaccuracy of the BJH method, only the carbon aerogels

derived from the 10 g formulation gave results that were consistent with the 2D-NLDFT-HS method. Indeed, the material A_10 is the only one having a narrow PSD in the mesopores range (with peaks well located in Figure 5d). For all the other materials, the low volumes of mesopores as well as their very broad and dispersed character in terms of PSD make the application of the BJH method unsuitable and inconsistent with the results obtained with the NLDFT method.

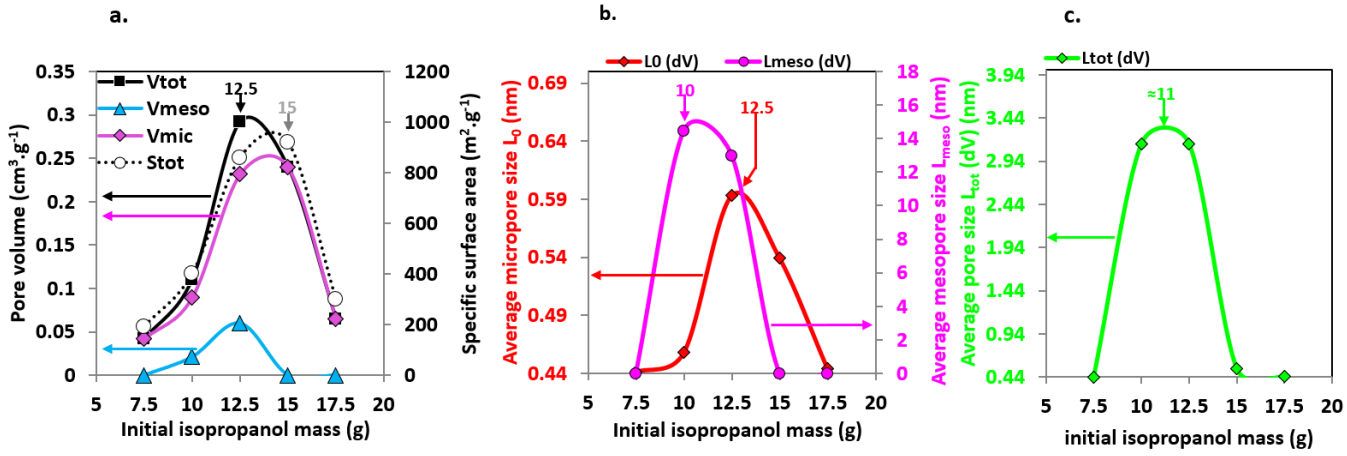

Figure 6. Pore texture of carbon aerogels as a function of the amount of isopropanol in the formulation: (a) total pore volume (V_{tot}), mesopore volume (V_{meso}), micropore volume (V_{μ}) and total specific area (S_{tot}); (b) average micropore (L_0) and mesopore (L_{meso}) sizes; and (c) total average pore size (L_{tot}). All the values were obtained using data from the PSD obtained by application of the NLDFT model. The pore sizes were calculated using volume (dV) ponderations.

Figure 6a shows that the maximum pore volume is reached for A_12.5 while the maximum of NLDFT surface area is reached for the A_15 material. Indeed, A_12.5 has a lower microporous volume than A_15, but the latter does not present any mesoporosity. Figure 6b shows that the largest average micropore size (0.59 nm) was obtained with A_12.5, while the maximum average mesopores size (15.5 nm) was for A_10. The optimum of average total pore size L_{tot} (around 3.4 nm, see Figure 6c) corresponds to A_10 and A_12.5. Therefore, the

material chosen as the most desirable for liquid-phase adsorption of organic molecules was the carbon aerogel A_12.5. This material indeed has the best balance between pore volume, surface area and pore size.

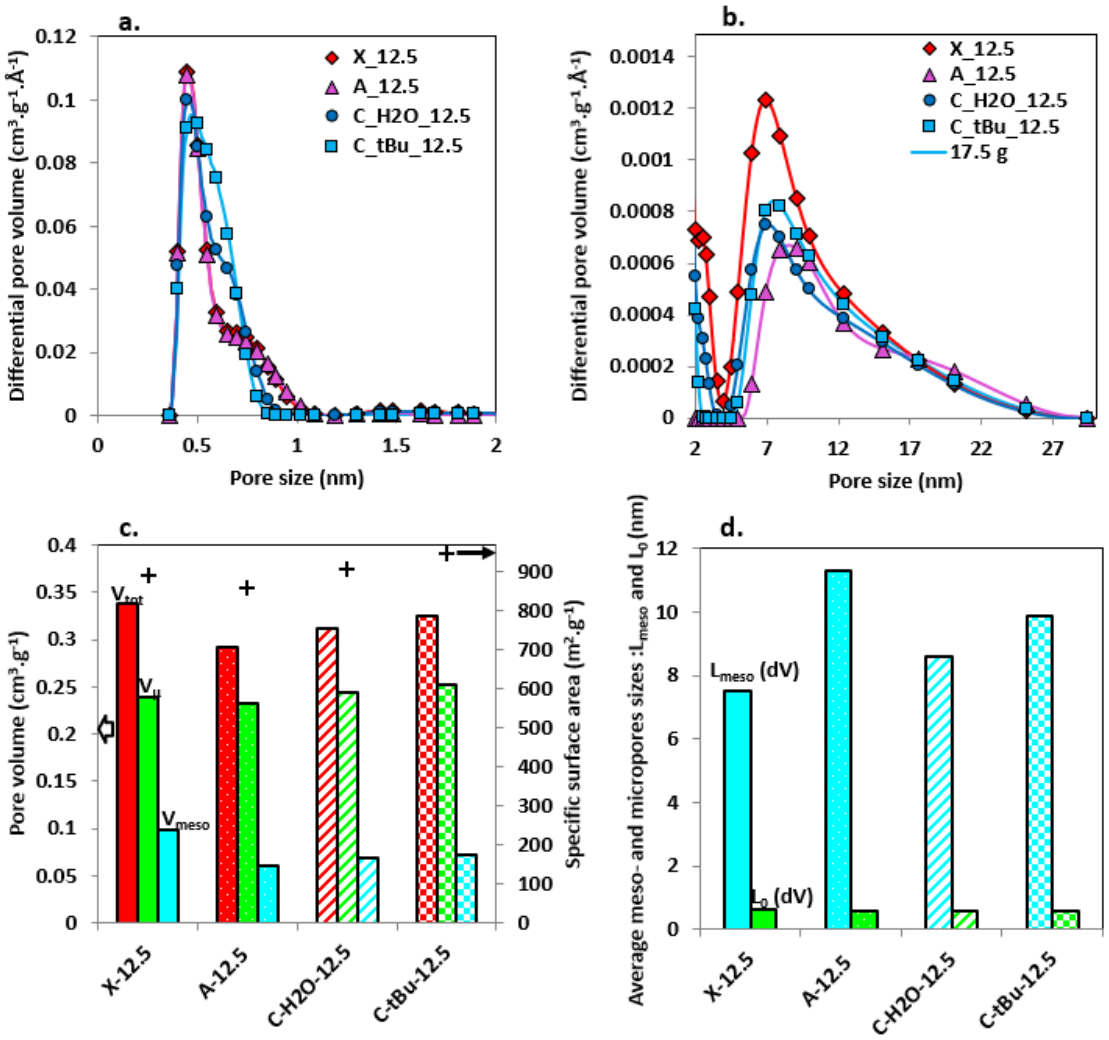

Figure 7. Pore textures of carbon xerogel, cryogel and aerogel derived from the formulation 12.5 g. Pore size distributions: (a) in the micropore range, and (b) in the mesopore range, according to NLDFT; (c) Total pore volumes (V_{tot}), microporous (V_{μ}), mesoporous volumes (V_{meso}) and NLDFT surface areas; (d) average mesopores (L_{meso}), micropore (L_0) and total average (L_{tot}) pore sizes.

When comparing the impact of the drying method for the same formulation 12.5 g, it can be noted that all the isotherms are type Ia-IV (Figure S4a). Even if the isotherms exhibit

similar adsorbed amounts for the different carbon gels, some differences can be seen. Surprisingly, the carbon aerogel had the lowest adsorbed volumes of all these carbon gels. According to the CO_2 adsorption isotherms (Figure S4b), the volumes of ultramicropores were similar whatever the drying mode. Figures 7a and 7b show that the PSDs of the carbon gels derived from the 12.5 g formulation are comparable despite the different ways of drying used for their organic precursors. These PSDs are indeed unimodal in the range of micropore sizes, have similar amplitudes, and the position of their peaks is located at 0.45-0.46 nm.

As for the aerogels (Figure 5c), the PSDs were narrow and very similar in shape, position and amplitude. The comparison of the main textural characteristics (total pore volume and specific surface area) of carbon aero-, xero-, and cryogels can be found in Figure 7c and in Table 3. First, the specific surface areas are similar and in the range of 860 to 950 $m^2\ g^{-1}$. The same observation can be made on the total pore volumes, which are between 0.29 and 0.34 $cm^3\ g^{-1}$. Therefore, the drying method had a moderate effect on the textural properties of the final carbon materials. This is due to the essentially ultramicroporous nature of the texture of the gels. Indeed, in such a range of pore sizes, no menisci are formed during the drying step and, therefore, it is unlikely that a pore collapse mechanism could occur in such small pores. Figure 7d and Table 3 show the average pore size in the micro- and mesopores ranges. The carbon aerogel is the material that exhibited the highest average mesopores size.

Given the small differences in texture and considering the drying cost, the X_12.5 material was thus chosen to perform the MB adsorption tests.

3.1.6. Surface chemistry

Figure 8a shows the proton-binding curve, expressed in mmol of NaOH per gram of carbon gel, *Q*, obtained by treating the titration curve of X_12.5. The excellent fit obtained after application of the Saieus-pK-Dist software is also shown. Figure 8b presents the distribution of acidity constants f(pK_a) giving access to the pK_a and the quantification of the

587 acidic and basic functionalities. The curve f(pK_a) presents only two peaks with pK_a maxima at
588 3.03 and 11.15. The pK_a distribution shows the predominance of strongly basic species: 0.23
589 mmol/g at pK_a = 11.5, compared to 0.05 mmol/g of strong acidic surface groups, at pK_a =
590 3.03.

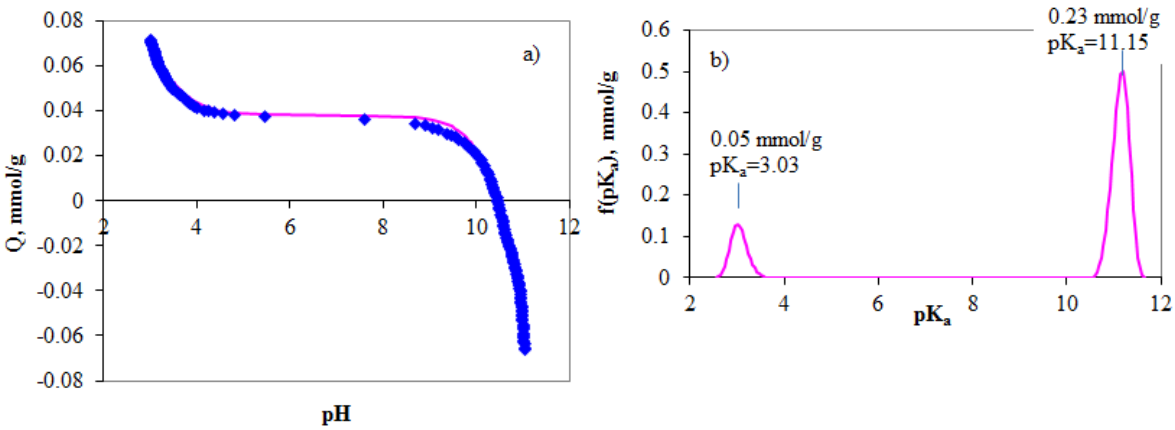

591

592 **Figure 8.** Results of potentiometric titration of the carbon xerogel X_12.5: (a) proton-binding
593 curve and (b) distribution of acidity constants.

594 Some surface groups, having a *pKa* beyond 10 (*pKa* = 11.15) can be noticed on the *pKa*
595 distribution. Such groups can be assimilated to phenol groups [94]. In a lesser extent, other
596 groups having *pKa* between 3 and 7, can also be noticed and are assimilated to carboxylic or
597 carboxylic anhydride groups (*pKa* = 3.03) [94].

598 3.2. MB adsorption properties

599 *3.2.1. Adsorption kinetics*

600 The pseudo-first and pseudo second order kinetic plots for the solutions containing initially
601 10 and 90 mg L^{-1} of MB (25°C) are presented in Figures 9a and 9b. The linear fit of the
602 pseudo-second order kinetic model led to a poor to fair correlation (R^2 in the 0.79-0.98 range)
603 while the pseudo-second order gave a much better determination coefficient (R^2 very close to
604 1). This allows concluding that the adsorption kinetics of MB on the X_12.5 carbon gel
605 follows a pseudo-second order. The low adsorption rates (presented in Table S2) are due to

606 the very small pore size of the material (L_0 around 0.62 nm and L_{tot} around 3 nm). Such
607 narrow pore sizes slow down the diffusion of MB molecules to their final adsorption site. The
608 initial rates, h_0, are respectively equal to 0.084 and 0.329 mg g^{-1} min^{-1} for the solutions
609 containing 10 and 90 mg L^{-1} of MB.

610 The diffusion of MB molecules follows three regimes, represented by 0), 1) and 2) in
611 Figure 9c. The first regime 0) is quite slow (slope slightly less than that given by regime 1)),
612 and might be due to the progressive impregnation of the carbon particles by the solution.
613 Indeed, it can be assumed that the penetration of the solvent (i.e., water) containing the MB
614 molecules is quite slow due the narrowness of the pores. The diffusion regime 1) is slightly
615 faster (K_D in the range of 0.517-1.405 mg g^{-1} $min^{-1/2}$) and the intercept of its linear equation is
616 equal to zero. A zero intercept means that the diffusional resistance (R_1) during this period is
617 almost inexistent. Thus, during this period, the molecules already adsorbed still do not slow
618 down the diffusion of the MB molecules in the liquid phase. In addition, during this second
619 period, the system is still very far from the equilibrium condition, and the MB concentration
620 remains quite high, which leads to this fast rate, compared to the next, adsorption, step
621 (regime 2)) [86].

622 After approximatively 200 min of adsorption, the diffusion rate decreased and switched
623 from regime 1) to regime 2). This transition occurred earlier (around 200 min) in the case of
624 the 90 mg L^{-1} MB solution than for the 10 mg L^{-1} MB solution (around 300 min). This is due
625 to a more important steric hindrance induced by the more important adsorbed amount in the
626 case of the 90 mg L^{-1} solution when compared to the 10 mg L^{-1}, and to a rarefaction of MB
627 molecules in the solution. Consequently, the diffusion rates decreased from 0.517 to 0.251 mg
628 g^{-1} $min^{-0.5}$ in the case of the 10 mg L^{-1} MB solution, and from 1.405 to 0.177 mg g^{-1} $min^{-0.5}$ in
629 the case of the 90 mg L^{-1} MB solution. A diffusion resistance (non-zero intercept) also
630 appeared in both cases.

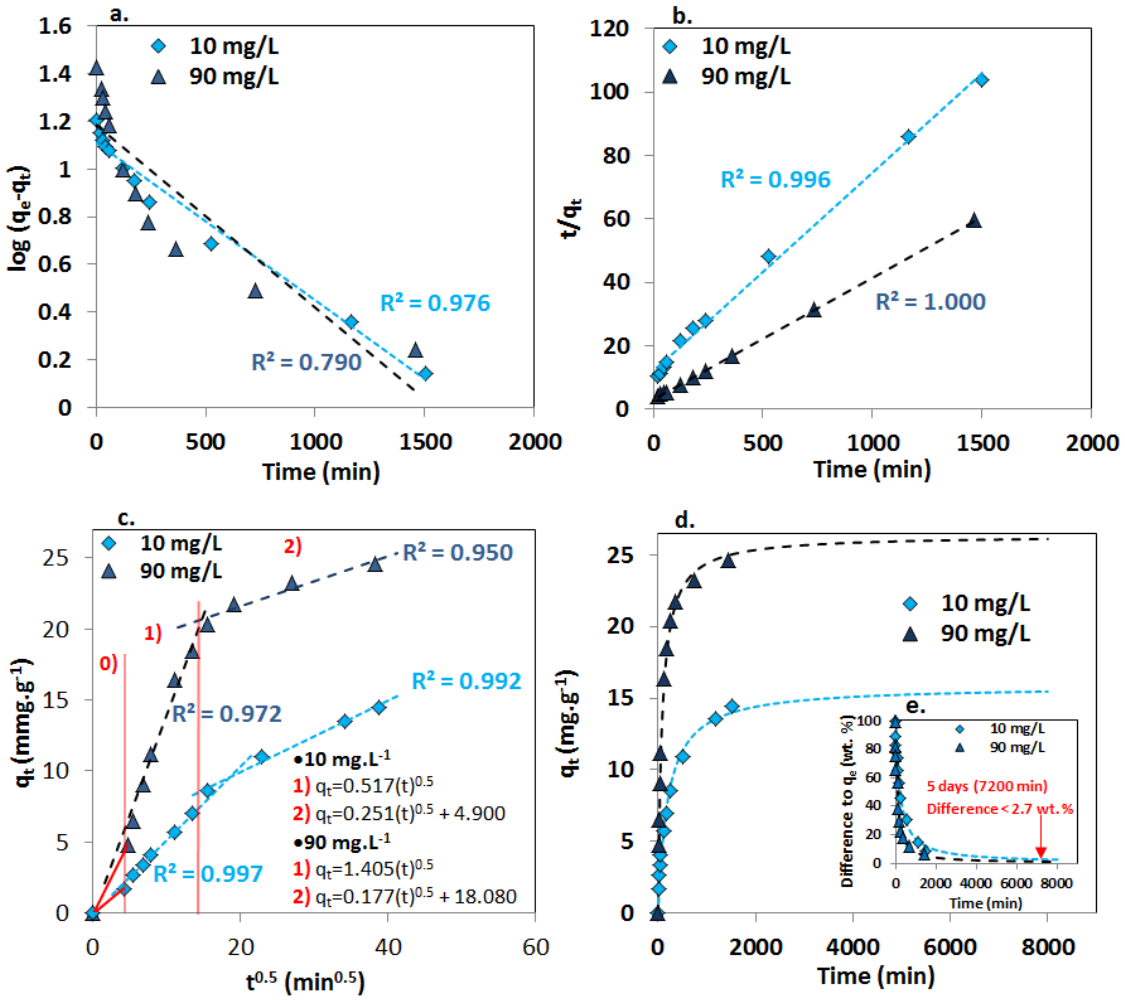

Figure 9. Adsorption kinetics of MB on X_12.5 carbon xerogel: (a) pseudo-first order plot, (b) pseudo-second order plot, (c) intra-particular diffusion plot, and (d) fit of the pseudo-second order to the adsorbed amount as a function of time for initial MB concentrations of 10 and 90 mg L^{-1} at 25°C; the inset (e) shows the difference between the two curves.

This diffusion resistance was higher when the initial concentration increased due to the faster initial adsorption rate and the higher adsorbed amount when the initial concentration was higher. The plot of adsorbed amount as a function of time and its modelling according to a pseudo second order kinetics show that, after 1500 min (25 h), the equilibrium was reached at least at 90 % (Figure 9d). Thus, in order to minimise the error on the equilibrium points, the duration of the adsorption experiment was fixed at 5 days. Such duration corresponds to an error of 2.7% on the equilibrium condition, which is acceptable compared to the combined

experimental errors on the dilutions, initial concentrations and sample weights. The parameters of the pseudo-first and pseudo-second order are given in Table S2.

The very narrow micropore size of the X_12.5 carbon gel explains the slow diffusion of MB molecules. Indeed, taking into account the molecular size of MB (≈ 1.70 × 0.74 ×0.33 nm), after rapid filling of the biggest pores, the MB molecules can only slide laterally in the smallest pores (ultramicropores) (Figure 10). In addition, and as explained before, the previously adsorbed molecules induce a steric hindrance effect and slow down the adsorption and diffusion process. Moreover, the methylene blue molecules should desolvate upon entering the narrowest pores. This necessary desolvation step hinders adsorption [95], and is this likely to slow down the adsorption process.

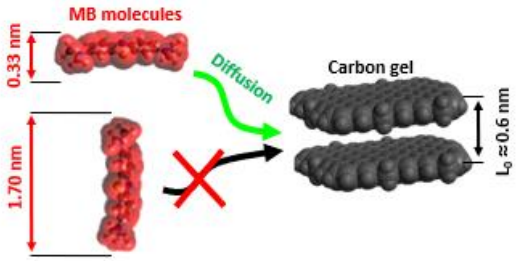

Figure 10. Schematic diffusion of methylene blue molecules within ultramicropores.

3.2.2. Adsorption at equilibrium

Figure 11a shows the MB adsorption isotherms on the X_12.5 carbon gel. A maximum adsorption capacity of 72.50 mg g^{-1} was measured at 45°C, and it decreased to 47.00 and 34.00 mg L^{-1} when the temperature decreased to 25°C and 15°C, respectively. When the adsorption is thermodynamically favourable (the free enthalpy of displacement is negative [96]), this type of behaviour possibly indicates an endothermal process associated with entropy-driven adsorption and displacement [96, 97]. Table S3 shows the Langmuir,

Freundlich and Sips parameters. Sips model best fitted the experimental data (R^2 in the range of 0.979-0.997).

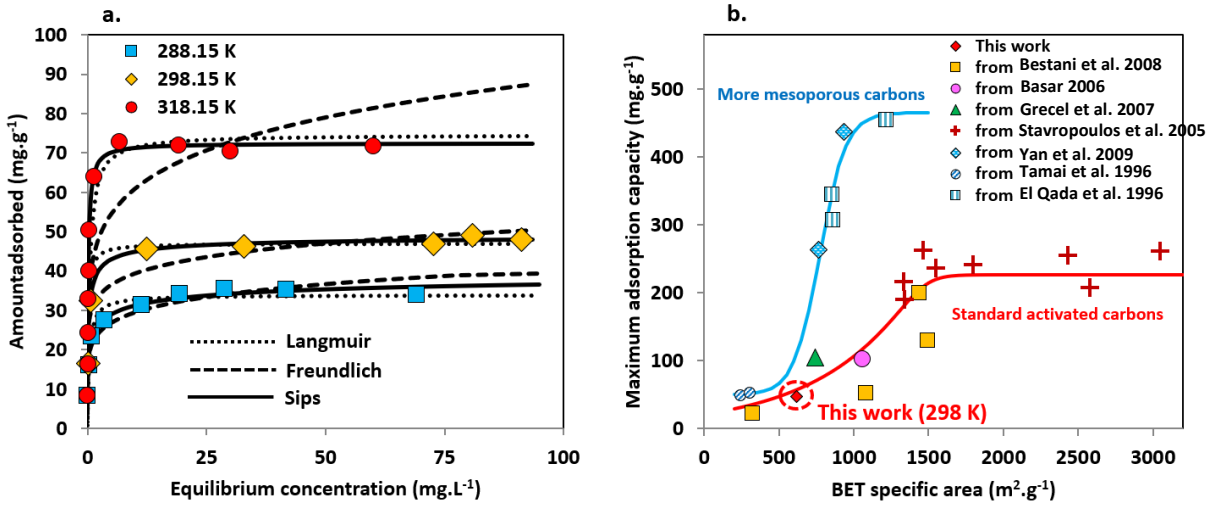

Figure 11. (a) Methylene blue adsorption isotherms of the X_12.5 carbon xerogel carried out at different temperatures. (b) Methylene blue adsorption capacities (15°C – 45°C) of various carbons from the literature [98-104] as a function of BET area, where the solid lines are sigmoid functions.

As the temperature increased, the quality of the fit (both through R^2 and χ^2 values) of the Langmuir model increased while that of the Freundlich model got worse (Table S3). This transition from Freundlich to Langmuir model is explained by the fact that at higher temperatures, the maximum capacity of the material is reached for lower equilibrium concentration. Therefore, the higher the temperature, the narrower the knee of the adsorption isotherm is. Typically, the Freundlich isotherm model gives poor results when the material is close to the saturation capacity and when the filling of adsorption sites increases very fast with the equilibrium concentration. The fitting parameters of the three models are given in Table S3.

The comparison of the adsorption capacity of X_12.5 with other carbonaceous materials is presented in Figure 11b. The X_12.5 carbon gel fits well the trend of classic activated

carbons. Unlike most of the materials presented in this Figure, X_12.5 was synthesised without any activation or doping. In addition, the precursor consisted of a low-value product (phenolic oil) that may be considered as waste. Materials with mesoporosity exhibit higher capacities than usual microporous carbons. Wider pores could allow a better organisation of the adsorbed MB molecules and, consequently, better packing on the adsorbent surface. In addition, the average pore size (around 0.62 nm) allows the adsorption of a single MB molecule (1.70 × 0.74 × 0.33 nm) between the two walls of a slit-shaped ultramicropore. Such an adsorption mechanism, due to the possible permanent pore blocking, decreases the potential maximum adsorption capacity of the material.

3.2.3. Adsorption thermodynamics

The use of equation (13) gives access to the equilibrium constant. We chose an equilibrium centration equal to 1 mg L^{-1} MB ($c_e \approx 3.13\ 10^{-3}$ mol L^{-1}) and we used the Sips model to obtain the adsorbed concentration, c_{ads}, for the three isotherms. c_{ads} was simply obtained by dividing the number of moles of adsorbed MB by the volume of the solution. Table 4 shows the free enthalpies of adsorption as well as the estimated equilibrium constants calculated using equation 13.

Table 4. Equilibrium constants from different estimations and their associated free enthalpies.

	Temperature		
	15°C	25°C	45°C
$K = c_{ads}/c_e$ (dimensionless)	14.95	24.10	30.89
ΔG_{ads} (kJ mol^{-1})	-6.5	-7.9	-9.1

The good quality of the linear regression allows calculating the changes of enthalpy (ΔH_{ads}) and entropy (ΔS_{ads}) during the adsorption process (equation (14)). The value of ΔH_{ads} was close to 17 kJ mol^{-1}, while that of ΔS_{ads} was equal to 83 J mol^{-1} K^{-1}. The use of the

isosteric method (equation (16)) on Sips isotherms (equation (10)), combined to the enthalpy/entropy compensation principle (equation (18)), led to similar values. The latter were indeed close to 25 kJ mol^{-1} when considering the adsorption enthalpy while the adsorption entropy was close to 83 J mol^{-1} K^{-1}. The positive values of entropy can be analysed as an increase in the disorder of the solvent phase due to desorption of water molecules from the carbon surface or to desolvation of MB molecules. However, the observation of a single value of adsorption enthalpy or entropy, at a given equilibrium concentration, is not enough to fully understand the adsorption process. The assessment of the thermodynamic parameters should be carried out over the entire range of coverage.

Figure 12a presents the adsorption (or displacement) enthalpies (at 298 k) from both the isosteric method and the Van't Hoff equation. Above the range of low fractional coverage (i.e., at $\theta > 0.2$), the isosteric heat becomes negative (and therefore ΔH_{ads} becomes positive). Thus, it can be assumed that the overall displacement process (water desorption and MB adsorption) is exothermal within the range of low coverage while at high coverage, the aforementioned process is endothermal.

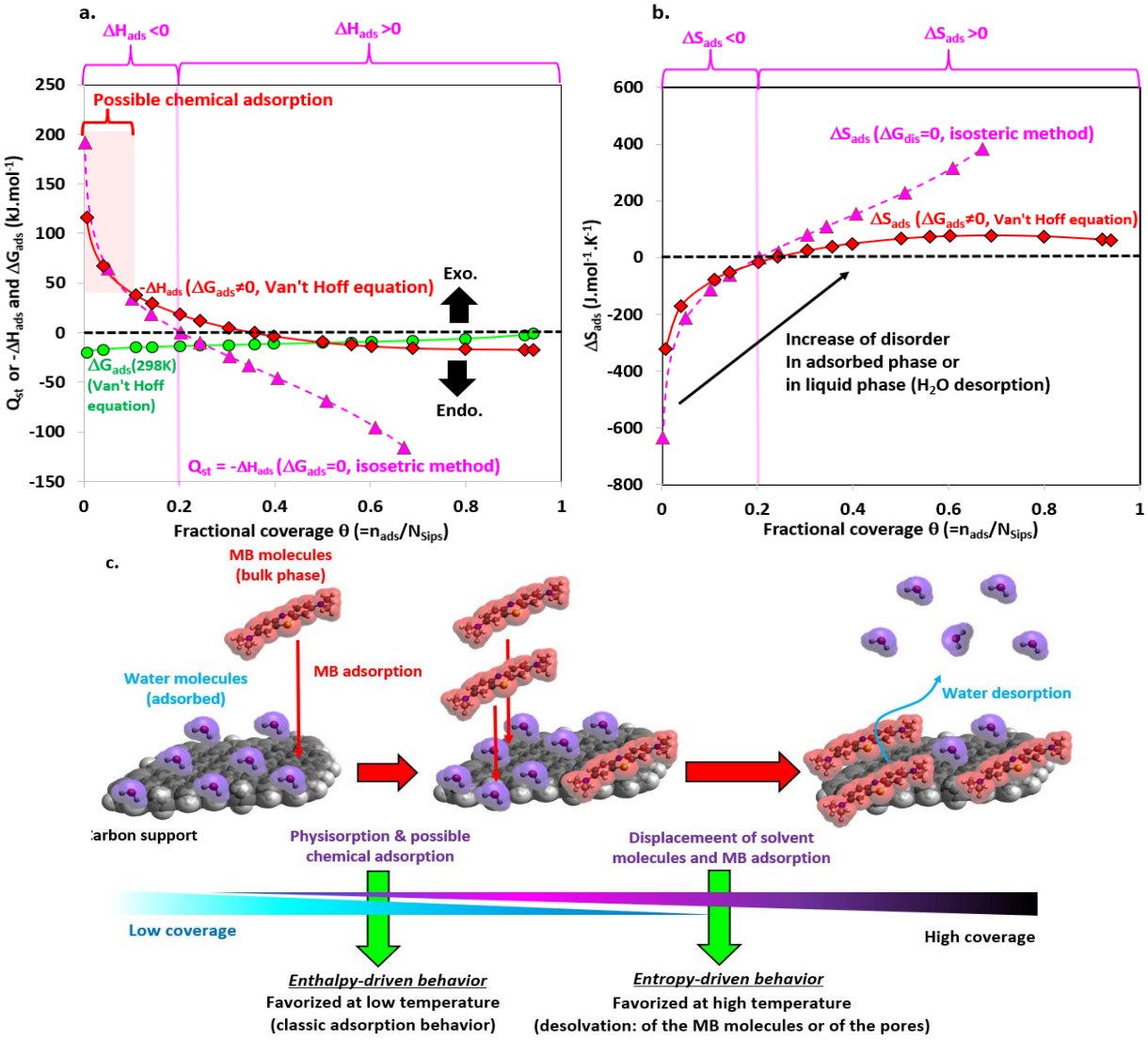

Figure 12. (a) Enthalpy and Gibbs free energy; (b) entropy; and (c) supposed mechanism of methylene blue adsorption at 24°C on the X_12.5 carbon gel (results obtained using either the isosteric method or the Van't Hoff equation).

As expected from the enthalpy/entropy compensation principle (isosteric method only), an opposite behaviour is observed for isosteric adsorption entropies. The gradual increase in isosteric entropy of adsorption (or displacement) could be analysed as an increase in water desorption from the carbon surface as the adsorption proceeds. Thus, the higher the coverage by MB, the higher water desorption, which initially covers the entire carbon surface.

Consequently, the MB adsorption and packing, which should make adsorption improbable, do not balance the increase in entropy, induced by water desorption and the possible desolvation of MB molecules. Therefore, at low coverage, MB adsorption follows a classic enthalpy-driven process, which is possibly due to strong physisorption or even chemical adsorption on specific sites. Above the low coverage region ($\theta > 0.2$), the adsorption of MB on X_12.5 becomes an entropy-driven process, in which the desolvation of MB molecules and water desorption from the carbon surface are favoured at high temperature. Such a transition from enthalpy-driven process to entropy-driven process has been evidenced by other authors for the adsorption of n-butanol/water and benzene/n-heptane on carbon black and silica gel, respectively [96, 105].

At low coverage, thermodynamic parameters thus obtained, either by the isosteric method or by the Van't Hoff equation (ΔH_{ads} and ΔS_{ads}), follow the same evolution depending on coverage (Figure 12a and 12b). At high coverage, the quantities obtained from the isosteric method seem to diverge towards infinite values while those obtained from the Van't Hoff equation seem to converge to 0. The aforementioned specific adsorption sites are, most likely, the heteroatoms that are present in the surface groups like phenols (i.e., pK_a = 11.15) or carboxylic and carboxylic anhydride groups (i.e. *pKa* =3.03). On these specific sites, chemical adsorption and highly polarised physisorption can take place. Indeed, the MB molecule has a permanent dipole like the aforementioned surface groups. Consequently, Keesom forces, complementary to chemisorption, might play a major role in adsorption in this low range of coverage. A possible adsorption mechanism of the MB molecules on this carbon surface is proposed in Figure 12c.

In order to verify the validity of the estimation of the thermodynamic parameters, a comparison was made with different materials (Figure 13). The calculated values, using the

isosteric method or the Van't Hoff equation, are similar to those found in the literature. Such similarities show the robustness of the two methods to compare thermodynamic data.

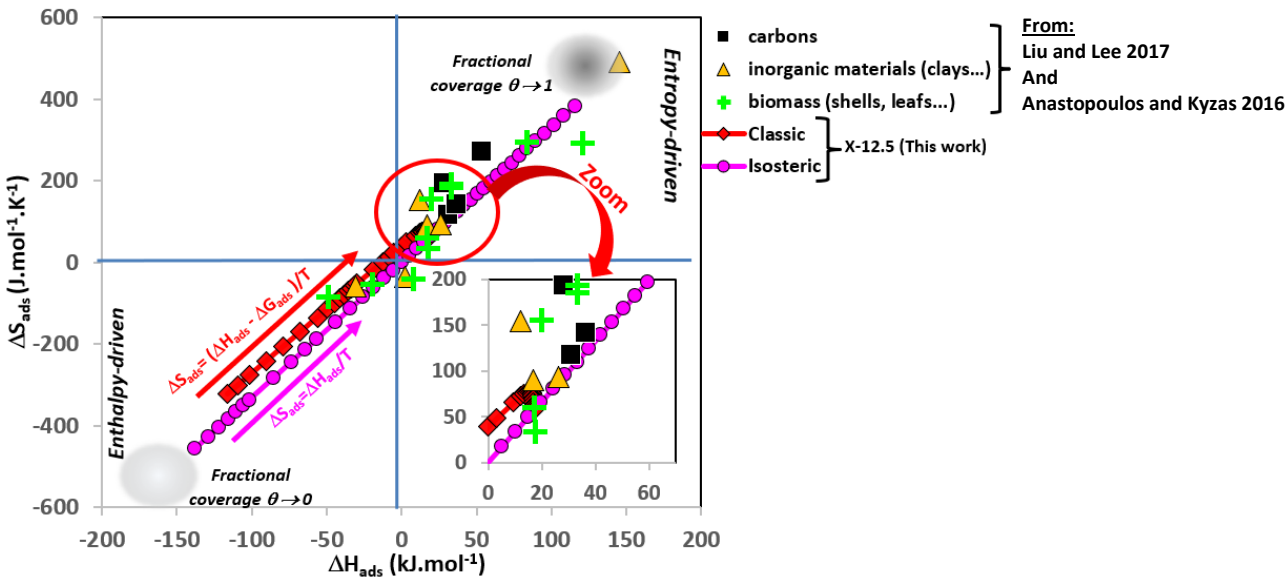

Figure 13. Entropies versus enthalpies of adsorption of methylene blue on the X_12.5 carbon gel, obtained by the isosteric method (●) or the Van't Hoff equation (■) compared with some data from the literature [106, 107].

4. Conclusion

The use of phenolic oil (PO) combined with para-toluenesulphonic-acid (PTSA), paraformaldehyde (PF) and isopropanol (IPA) as a solvent, allowed synthesising organic solvogels. The investigations were carried out using a formulation containing 3.123 g of PF, 0.64 g of PTSA, 10 g of PO and different amounts of IPA. The almost exclusively ultramicroporous texture allowed obtaining similar textural properties whatever the drying mode (supercritical drying, cryodesiccation, or classical convective drying). The formulation with 12.5 g of IPA was selected as the best, and a carbon xerogel was selected to test and investigate methylene blue (MB) adsorption.

This carbon xerogel had a BET area of 620 m^2 g^{-1} while its NLDFT surface area was 891 m^2 g^{-1}. MB adsorption was slow due to the very narrow pores (L_0 = 0.62 nm), and the adsorption capacity of the carbon at 25°C was estimated at 47.00 mg g^{-1}, in good agreement with the literature. The Sips model was the best to fit the MB adsorption isotherms, and the calculation of the thermodynamic parameters using both conventional and isosteric methods led to positives values of the change of entropy (at c_e = 1 mg L^{-1}: 83 J mol^{-1} K^{-1}), suggesting that the adsorption of MB in these materials is driven by entropy above a 20% of coverage. Such entropy-driven behaviour can be explained either by the desolvation of the MB molecules when they enter the smallest pores or by water desorption from the carbon surface. Below such limit coverage, the analysis of the thermodynamic parameters suggests that the adsorption process is driven by enthalpy. Such phenomenon is probably due to specific adsorption sites, as heteroatoms or defects, on the carbon surface.

This study thus reported the first successful acid-catalysed synthesis of gel based on PO published so far, the only previous work on a similar topic concerning base-catalysed gels, hence with different characteristics. The crosslinking agent, PF, can also be considered as a by-product of the formaldehyde industry. Therefore, the use of PO and PF can be seen as a win-win situation and as an attempt to recover these 'wastes' and integrate them into a circular economy. The adsorption capacities and the kinetics of the materials synthesised here might be improved further by tuning their textural properties. For instance, an activation step or a preliminary mesostructuration would probably increase the porous volume as well as the accessibility of the pores. As the precursor is PO, an industrial by-product, such steps could be affordable from an environmental and energy perspective.

ACKNOWLEDGMENTS

Authors gratefully acknowledge the funding from the Research Fund for Coal and Steel (RFCS) of the European Union (EU) under grant agreement No 709741. This study was also partly supported by TALiSMAN project, funded by FEDER (2019-000214).

References

[1] R.W. Pekala, D.W. Schaefer, STRUCTURE OF ORGANIC AEROGELS .1. MORPHOLOGY AND SCALING, Macromolecules 26(20) (1993) 5487-5493.

[2] R.W. Pekala, ORGANIC AEROGELS FROM THE POLYCONDENSATION OF RESORCINOL WITH FORMALDEHYDE, Journal of Materials Science 24(9) (1989) 3221-3227.

[3] R.W. Pekala, C.T. Alviso, F.M. Kong, S.S. Hulsey, AEROGELS DERIVED FROM MULTIFUNCTIONAL ORGANIC MONOMERS, Journal of Non-Crystalline Solids 145(1-3) (1992) 90-98.

[4] L. Pilato, Phenolic resins: 100 Years and still going strong, Reactive & Functional Polymers 73(2) (2013) 270-277.

[5] D.C. Wu, R.W. Fu, Z.Q. Sun, Z.Q. Yu, Low-density organic and carbon aerogels from the sol-gel polymerization of phenol with formaldehyde, Journal of Non-Crystalline Solids 351(10-11) (2005) 915-921.

[6] D.H. Long, J. Zhang, J.H. Yang, Z.J. Hu, G. Cheng, X.M. Liu, R. Zhang, L. Zhan, W.M. Qiao, L.C. Ling, Chemical state of nitrogen in carbon aerogels issued from phenol-melamine-formaldehyde gels, Carbon 46(9) (2008) 1259-1262.

[7] C. Scherdel, G. Reichenauer, Carbon xerogels synthesized via phenol-formaldehyde gels, Microporous and Mesoporous Materials 126(1-2) (2009) 133-142.

[8] N. Job, C.J. Gommes, R. Pirard, J.P. Pirard, Effect of the counter-ion of the basification agent on the pore texture of organic and carbon xerogels, Journal of Non-Crystalline Solids 354(40-41) (2008) 4698-4701.

[9] F. Carrasco-Marin, D. Fairen-Jimenez, C. Moreno-Castilla, Carbon aerogels from gallic acid-resorcinol mixtures as adsorbents of benzene, toluene and xylenes from dry and wet air under dynamic conditions, Carbon 47(2) (2009) 463-469.

[10] Y.D. Zhu, H.Q. Hu, W.C. Li, H.X. Zhao, Preparation of cresol-formaldehyde carbon aerogels via drying aquagel at ambient pressure, Journal of Non-Crystalline Solids 352(30-31) (2006) 3358-3362.

[11] S. Schaefer, V. Fierro, A. Szczurek, M.T. Izquierdo, A. Celzard, Physisorption, chemisorption and spill-over contributions to hydrogen storage, International Journal of Hydrogen Energy 41(39) (2016) 17442-17452.

[12] A. Szczurek, G. Amaral-Labat, V. Fierro, A. Pizzi, A. Celzard, The use of tannin to prepare carbon gels. Part II. Carbon cryogels, Carbon 49(8) (2011) 2785-2794.

[13] A. Szczurek, G. Amaral-Labat, V. Fierro, A. Pizzi, E. Masson, A. Celzard, The use of tannin to prepare carbon gels. Part I: Carbon aerogels, Carbon 49(8) (2011) 2773-2784.

[14] L.I. Grishechko, G. Amaral-Labat, V. Fierro, A. Szczurek, B.N. Kuznetsov, A. Celzard, Biosourced, highly porous, carbon xerogel microspheres, Rsc Advances 6(70) (2016) 65698-65708.

[15] A. Szczurek, G. Amaral-Labat, V. Fierro, A. Pizzi, A. Celzard, Chemical activation of tannin-based hydrogels by soaking in KOH and NaOH solutions, Microporous and Mesoporous Materials 196 (2014) 8-17.

[16] A. Szczurek, G. Amaral-Labat, V. Fierro, A. Pizzi, A. Celzard, Iop, New families of carbon gels based on natural resources, Names10: New Achievements in Materials and Environmental Sciences2013.

[17] L.I. Grishechko, G. Amaral-Labat, A. Szczurek, V. Fierro, B.N. Kuznetsov, A. Celzard, Lignin-phenol-formaldehyde aerogels and cryogels, Microporous and Mesoporous Materials 168 (2013) 19-29.

[18] L.I. Grishechko, G. Amaral-Labat, A. Szczurek, V. Fierro, B.N. Kuznetsov, A. Pizzi, A. Celzard, New tannin-lignin aerogels, Industrial Crops and Products 41 (2013) 347-355.

[19] D.C. Wu, R.M. Fu, Synthesis of organic and carbon aerogels from phenol-furfural by two-step polymerization, Microporous and Mesoporous Materials 96(1-3) (2006) 115-120.

[20] R. Zhang, Y.G. Lu, Q.H. Meng, L. Zhan, G.P. Wu, K.X. Li, L.C. Ling, On porosity of carbon aerogels from sol-gel polymerization of phenolic novolak and furfural, Journal of Porous Materials 10(1) (2003) 57-68.

[21] D.C. Wu, R.W. Fu, Fabrication and physical properties of organic and carbon aerogel derived from phenol and furfural, Journal of Porous Materials 12(4) (2005) 311-316.
[22] D.C. Wang, L.J. Jin, Y. Li, B.Y. Wei, D.M. Yao, T.T. Wang, H.Q. Hu, Integrated process of coal tar upgrading and in-situ reduction of Fe2O3, Fuel Processing Technology 191 (2019) 20-28.
[23] Y.G. Wang, Z.S. Niu, J. Shen, P. Li, Y.X. Niu, W. Zhao, X.Y. Wei, Formation of benzene polycarboxylic acids using alkali-oxygen oxidation of coal-tar pitch pre-treated by extraction and air-blowing, Fuel Processing Technology 185 (2019) 100-105.
[24] D.L. Wang, D.M. Wang, J. Yu, Z.H. Chen, Y.J. Li, S.Q. Gao, Role of alkali sodium on the catalytic performance of red mud during coal pyrolysis, Fuel Processing Technology 186 (2019) 81-87.
[25] M.Y. Wang, L.J. Jin, Y. Li, J.N. Lv, B.Y. Wei, H.Q. Hu, In-situ catalytic upgrading of coal pyrolysis tar coupled with CO2 reforming of methane over Ni-based catalysts, Fuel Processing Technology 177 (2018) 119-128.
[26] D.Q. Fu, X.H. Li, W.Y. Li, J. Feng, Catalytic upgrading of coal pyrolysis products over bio-char, Fuel Processing Technology 176 (2018) 240-248.
[27] A. Sanchez-Sanchez, M.T. Izquierdo, S. Mathieu, G. Medjahdi, V. Fierro, A. Celzard, Activated carbon xerogels derived from phenolic oil: Basic catalysis synthesis and electrochemical performances, Fuel Processing Technology (2020).
[28] E. Garcia-Diez, S. Schaefer, A. Sanchez -Sanchez, A. Celzard, V. Fierro, M.M. Maroto-Valer, S. Garcia, Novel Porous Carbons Derived from Coal Tar Rejects: Assessment of the Role of Pore Texture in CO2 Capture under Realistic Postcombustion Operating Temperatures, Acs Applied Materials & Interfaces 11(40) (2019) 36789-36799.
[29] R. Banerjee, K. Patil, K.C. Khilar, Studies on phenol-formaldehyde gel formation at a high temperature and at different pH, Canadian Journal of Chemical Engineering 84(3) (2006) 328-337.
[30] S.R. Mukai, C. Tamitsuji, H. Nishihara, H. Tamon, Preparation of mesoporous carbon gels from an inexpensive combination of phenol and formaldehyde, Carbon 43(12) (2005) 2628-2630.
[31] W.C. Li, S.C. Guo, Preparation of low-density carbon aerogels from a cresol/formaldehyde mixture, Carbon 38(10) (2000) 1520-1523.
[32] D.H. Long, J. Zhang, J.H. Yang, Z.J. Hu, T.Q. Li, G. Cheng, R. Zhang, L.C. Ling, Preparation and microstructure control of carbon aerogels produced using m-cresol mediated sol-gel polymerization of phenol and furfural, New Carbon Materials 23(2) (2008) 165-170.
[33] W.C. Li, H. Probstle, J. Fricke, Electrochemical behavior of mixed CmRF based carbon aerogels as electrode materials for supercapacitors, Journal of Non-Crystalline Solids 325(1-3) (2003) 1-5.
[34] R. Zhang, W. Li, K.X. Li, C.X. Lu, L. Zhan, L.C. Ling, Effect of concentration of reactants on porosity of hydrogels, organic and carbon aerogels, Microporous and Mesoporous Materials 72(1-3) (2004) 167-173.
[35] Y.D. Zhu, H.Q. Hu, W.C. Li, X.Y. Zhang, Cresol-formaldehyde based carbon aerogel as electrode material for electrochemical capacitor, Journal of Power Sources 162(1) (2006) 738-742.
[36] W.C. Li, G. Reichenauer, J. Fricke, Carbon aerogels derived from cresol-resorcinol-formaldehyde for supercapacitors, Carbon 40(15) (2002) 2955-2959.
[37] H.L. Allen, E.G. Kerr, Process of producing indene modified phenol formaldehyde resins, US patent No. US2540641A, 1951.
[38] F.J. Soday, Process for the production of an indene phenol, US Patent No. US2423415A, 1947.
[39] H.R. Bailey, F.W. Corkery, Coumarone-indene resin, US Patent No. US2285416A, 1942.
[40] F.W. Corkery, Coumarone-indene resin, US patent No. US2285417A, 1942.
[41] L.M. Geiger, Alcohol-soluble phenol-modified coumarone-indene resin, US patent No. US2466889A, 1949.
[42] J.J. Freeman, J.R. Patterson, H.B. Wheeler, Process for producing phenol-modified coumarone-indene type resins, US patent No. US3032533A, 1962.
[43] G.Y. Pan, Z.J. Du, C. Zhang, C. Li, X.P. Yang, H.Q. Li, Synthesis, characterization, and properties of novel novolac epoxy resin containing naphthalene moiety, Polymer 48(13) (2007) 3686-3693.
[44] Y.F. Duann, T.M. Liu, K.C. Cheng, W.F. Su, Thermal stability of some naphthalene- and phenyl-based epoxy resins, Polymer Degradation and Stability 84(2) (2004) 305-310.

[45] T. Nemoto, G.I. Konishi, Synthesis and properties of new organosoluble alkoxylated naphthalene-based novolacs preparaed by addition-condensation of mono- or di-alkoxynaphthalene with formaldehyde, Polymer Journal 40(7) (2008) 651-656.
[46] R.W. Fu, B. Zheng, J. Liu, M.S. Dresselhaus, G. Dresselhaus, J.H. Satcher, T.E. Baumann, The fabrication and characterization of carbon aerogels by gelation and supercritical drying in isopropanol, Advanced Functional Materials 13(7) (2003) 558-562.
[47] V. Fierro, G. Muniz, A.H. Basta, H. El-Saied, A. Celzard, Rice straw as precursor of activated carbons: Activation with ortho-phosphoric acid, Journal of Hazardous Materials 181(1-3) (2010) 27-34.
[48] S. Shevade, R.G. Ford, Use of synthetic zeolites for arsenate removal from pollutant water, Water Research 38(14-15) (2004) 3197-3204.
[49] J. Sanchez-Martin, J. Beltran-Heredia, P. Gibello-Perez, Adsorbent biopolymers from tannin extracts for water treatment, Chemical Engineering Journal 168(3) (2011) 1241-1247.
[50] F. Banat, S. Al-Asheh, R. Al-Ahmad, F. Bni-Khalid, Bench-scale and packed bed sorption of methylene blue using treated olive pomace and charcoal, Bioresource Technology 98(16) (2007) 3017-3025.
[51] F. Pagnanelli, S. Mainelli, F. Veglio, L. Toro, Heavy metal removal by olive pomace: biosorbent characterisation and equilibrium modelling, Chemical Engineering Science 58(20) (2003) 4709-4717.
[52] G. Crini, Recent developments in polysaccharide-based materials used as adsorbents in wastewater treatment, Progress in Polymer Science 30(1) (2005) 38-70.
[53] V. Fierro, G. Muniz, G. Gonzalez-Sanchez, M.L. Ballinas, A. Celzard, Arsenic removal by iron-doped activated carbons prepared by ferric chloride forced hydrolysis, Journal of Hazardous Materials 168(1) (2009) 430-437.
[54] G. Muniz, V. Fierro, A. Celzard, G. Furdin, G. Gonzalez-Sanchez, M.L. Ballinas, Synthesis, characterization and performance in arsenic removal of iron-doped activated carbons prepared by impregnation with Fe(III) and Fe(II), Journal of Hazardous Materials 165(1-3) (2009) 893-902.
[55] N. Fiol, I. Villaescusa, M. Martinez, N. Miralles, J. Poch, J. Serarols, Sorption of Pb(II), Ni(II), Cu(II) and Cd(II) from aqueous solution by olive stone waste, Separation and Purification Technology 50(1) (2006) 132-140.
[56] R. Acosta, V. Fierro, A.M. de Yuso, D. Nabarlatz, A. Celzard, Tetracycline adsorption onto activated carbons produced by KOH activation of tyre pyrolysis char, Chemosphere 149 (2016) 168-176.
[57] T. Selmi, A. Sanchez-Sanchez, P. Gadonneix, J. Jagiello, M. Seffen, H. Sammouda, A. Celzard, V. Fierro, Tetracycline removal with activated carbons produced by hydrothermal carbonisation of Agave americana fibres and mimosa tannin, Industrial Crops and Products 115 (2018) 146-157.
[58] S.C.R. Marques, A.S. Mestre, M. Machuqueiro, A.Z. Gotvajn, M. Marinsek, A.P. Carvalho, Apple tree branches derived activated carbons for the removal of beta-blocker atenolol, Chemical Engineering Journal 345 (2018) 669-678.
[59] L.B. Khalil, Adsorption characteristics of activated carbon obtained from rice husks by treatment with phosphoric acid, Adsorption Science & Technology 13(5) (1996) 317-325.
[60] J. Ghasemi, S. Asadpour, Thermodynamics' study of the adsorption process of methylene blue on activated carbon at different ionic strengths, Journal of Chemical Thermodynamics 39(6) (2007) 967-971.
[61] A. Castro-Muniz, S. Lorenzo-Fierro, A. Martinez-Alonso, J.M.D. Tascon, V. Fierro, F. Suarez-Garcia, J.I. Paredes, Ordered mesoporous carbons obtained from low-value coal tar products for electrochemical energy storage and water remediation, Fuel Processing Technology 196 (2019).
[62] A.K. Meena, G.K. Mishra, P.K. Rai, C. Rajagopal, P.N. Nagar, Removal of heavy metal ions from aqueous solutions using carbon aerogel as an adsorbent, Journal of Hazardous Materials 122(1-2) (2005) 161-170.
[63] M. Sanchez-Polo, J. Rivera-Utrilla, E. Salhi, U. von Gunten, Removal of bromide and iodide anions from drinking water by silver-activated carbon aerogels, Journal of Colloid and Interface Science 300(1) (2006) 437-441.

[64] Y. Liu, Is the Free Energy Change of Adsorption Correctly Calculated?, Journal of Chemical and Engineering Data 54(7) (2009) 1981-1985.
[65] H. Gao, L. Ding, H. Bai, A.H. Liu, S.Z. Li, L. Li, Pitch-based hyper-cross-linked polymers with high performance for gas adsorption, Journal of Materials Chemistry A 4(42) (2016) 16490-16498.
[66] L.X. Tan, B. Tan, Hypercrosslinked porous polymer materials: design, synthesis, and applications, Chemical Society Reviews 46(11) (2017) 3322-3356.
[67] M. Sultania, J.S.P. Rai, D. Srivastava, Studies on the synthesis and curing of epoxidized novolac vinyl ester resin from renewable resource material, European Polymer Journal 46(10) (2010) 2019-2032.
[68] E. Fitzer, W. Schafer, EFFECT OF CROSSLINKING ON FORMATION OF GLASSLIKE CARBONS FROM THERMOSETTING RESINS, Carbon 8(3) (1970) 353-&.
[69] N. Job, R. Pirard, J. Marien, J.P. Pirard, Porous carbon xerogels with texture tailored by pH control during sol-gel process, Carbon 42(3) (2004) 619-628.
[70] N. Job, A. Thery, R. Pirard, J. Marien, L. Kocon, J.N. Rouzaud, F. Beguin, J.P. Pirard, Carbon aerogels, cryogels and xerogels: Influence of the drying method on the textural properties of porous carbon materials, Carbon 43(12) (2005) 2481-2494.
[71] G. Amaral-Labat, A. Szczurek, V. Fierro, E. Masson, A. Pizzi, A. Celzard, Impact of depressurizing rate on the porosity of aerogels, Microporous and Mesoporous Materials 152 (2012) 240-245.
[72] J. Jagiello, J. Kenvin, J.P. Olivier, A.R. Lupini, C.I. Contescu, Using a New Finite Slit Pore Model for NLDFT Analysis of Carbon Pore Structure, Adsorption Science & Technology 29(8) (2011) 769-780.
[73] J. Jagiello, J.P. Olivier, 2D-NLDFT adsorption models for carbon slit-shaped pores with surface energetical heterogeneity and geometrical corrugation, Carbon 55 (2013) 70-80.
[74] S. Schaefer, V. Fierro, M.T. Izquierdo, A. Celzard, Assessment of hydrogen storage in activated carbons produced from hydrothermally treated organic materials, International Journal of Hydrogen Energy 41(28) (2016) 12146-12156.
[75] S. Schaefer, G. Muniz, M.T. Izquierdo, S. Mathieu, M.L. Ballinas-Casarrubias, G. Gonzalez-Sanchez, A. Celzard, V. Fierro, Rice straw-based activated carbons doped with SiC for enhanced hydrogen adsorption, International Journal of Hydrogen Energy 42(16) (2017) 11534-11540.
[76] J. Rouquerol, P. Llewellyn, F. Rouquerol, Is the BET equation applicable to microporous adsorbents?, Characterization of Porous Solids Vii - Proceedings of the 7th International Symposium on the Characterization of Porous Solids (Cops-Vii), Aix-En-Provence, France, 26-28 May 2005 160 (2006) 49-56.
[77] M.M. Dubinin, V.A. Astakhov, DESCRIPTION OF ADSORPTION EQUILIBRIA OF VAPORS ON ZEOLITES OVER WIDE RANGES OF TEMPERATURE AND PRESSURE, Advances in Chemistry Series (102) (1971) 69-&.
[78] M.M. Dubinin, H.F. Stoeckli, HOMOGENEOUS AND HETEROGENEOUS MICROPORE STRUCTURES IN CARBONACEOUS ADSORBENTS, Journal of Colloid and Interface Science 75(1) (1980) 34-42.
[79] J. Jagiello, J. Kenvin, A. Celzard, V. Fierro, Enhanced resolution of ultra micropore size determination of biochars and activated carbons by dual gas analysis using N2 and CO2 with 2D-NLDFT adsorption models, Carbon 144 (2019) 206-215.
[80] J. Jagiello, C. Ania, J.B. Parra, C. Cook, Dual gas analysis of microporous carbons using 2D-NLDFT heterogeneous surface model and combined adsorption data of N-2 and CO2, Carbon 91 (2015) 330-337.
[81] E.P. Barrett, L.G. Joyner, P.P. Halenda, THE DETERMINATION OF PORE VOLUME AND AREA DISTRIBUTIONS IN POROUS SUBSTANCES .1. COMPUTATIONS FROM NITROGEN ISOTHERMS, Journal of the American Chemical Society 73(1) (1951) 373-380.
[82] M. Kruk, M. Jaroniec, A. Sayari, Application of large pore MCM-41 molecular sieves to improve pore size analysis using nitrogen adsorption measurements, Langmuir 13(23) (1997) 6267-6273.
[83] M. Jaroniec, L.A. Solovyov, Improvement of the Kruk-Jaroniec-Sayari method for pore size analysis of ordered silicas with cylindrical mesopores, Langmuir 22(16) (2006) 6757-6760.
[84] J. Jagiello, T.J. Bandosz, K. Putyera, J.A. Schwarz, DETERMINATION OF PROTON AFFINITY DISTRIBUTIONS FOR CHEMICAL-SYSTEMS IN AQUEOUS ENVIRONMENTS USING A STABLE

NUMERICAL-SOLUTION OF THE ADSORPTION INTEGRAL-EQUATION, Journal of Colloid and Interface Science 172(2) (1995) 341-346.
[85] Y.S. Ho, G. McKay, A comparison of chemisorption kinetic models applied to pollutant removal on various sorbents, Process Safety and Environmental Protection 76(B4) (1998) 332-340.
[86] K.C. Bedin, A.C. Martins, A.L. Cazetta, O. Pezoti, V.C. Almeida, KOH-activated carbon prepared from sucrose spherical carbon: Adsorption equilibrium, kinetic and thermodynamic studies for Methylene Blue removal, Chemical Engineering Journal 286 (2016) 476-484.
[87] S. Chowdhury, R. Mishra, P. Saha, P. Kushwaha, Adsorption thermodynamics, kinetics and isosteric heat of adsorption of malachite green onto chemically modified rice husk, Desalination 265(1-3) (2011) 159-168.
[88] A. Mianowski, W. Urbanczyk, Enthalpy-entropy compensation for isosteric state adsorption at near ambient temperatures, Adsorption-Journal of the International Adsorption Society 23(6) (2017) 831-846.
[89] I. Dekany, A. Zsednai, Z. Kiraly, K. Laszlo, L.G. Nagy, ENTHALPY OF DISPLACEMENT OF BINARY-LIQUID MIXTURES ON SOLID-SURFACES .1. ANALYSIS OF U-SHAPED ISOTHERMS, Colloids and Surfaces 19(1) (1986) 47-&.
[90] I. Johnson, R. Denoyel, J. Rouquerol, D.H. Everett, ADSORPTION AT THE LIQUID GRAPHITE INTERFACE - COMPARISON OF ENTHALPY DATA OBTAINED FROM 3 DIFFERENT METHODS, Colloids and Surfaces 49(1-2) (1990) 133-148.
[91] R. Denoyel, F. Rouquerol, J. Rouquerol, THERMODYNAMICS OF ADSORPTION FROM SOLUTION - EXPERIMENTAL AND FORMAL ASSESSMENT OF THE ENTHALPIES OF DISPLACEMENT, Journal of Colloid and Interface Science 136(2) (1990) 375-384.
[92] S.A. Al-Muhtaseb, J.A. Ritter, Preparation and properties of resorcinol-formaldehyde organic and carbon gels, Advanced Materials 15(2) (2003) 101-+.
[93] M. Thommes, K. Kaneko, A.V. Neimark, J.P. Olivier, F. Rodriguez-Reinoso, J. Rouquerol, K.S.W. Sing, Physisorption of gases, with special reference to the evaluation of surface area and pore size distribution (IUPAC Technical Report), Pure and Applied Chemistry 87(9-10) (2015) 1051-1069.
[94] B. Cagnon, S. Chatelain, T.F. de Oliveira, F. Versaveau, S. Delpeux, O. Chedeville, Adsorption of Phthalates on Activated Carbons in Monosolute Solution and in Mix Within Complex Matrices, Water Air and Soil Pollution 228(4) (2017).
[95] S.R. Sandeman, V.M. Gun'ko, O.M. Bakalinska, C.A. Howell, Y.S. Zheng, M.T. Kartel, G.J. Phillips, S.V. Mikhalovsky, Adsorption of anionic and cationic dyes by activated carbons, PVA hydrogels, and PVA/AC composite, Journal of Colloid and Interface Science 358(2) (2011) 582-592.
[96] Z. Kiraly, I. Dekany, ENTHALPY AND ENTROPY EFFECTS IN ADSORPTION AND DISPLACEMENT, Colloids and Surfaces 49(1-2) (1990) 95-101.
[97] M. Ghaedi, A.G. Nasab, S. Khodadoust, M. Rajabi, S. Azizian, Application of activated carbon as adsorbents for efficient removal of methylene blue: Kinetics and equilibrium study, Journal of Industrial and Engineering Chemistry 20(4) (2014) 2317-2324.
[98] B. Bestani, N. Benderdouche, B. Benstaali, M. Belhakem, A. Addou, Methylene blue and iodine adsorption onto an activated desert plant, Bioresource Technology 99(17) (2008) 8441-8444.
[99] C.A. Basar, Applicability of the various adsorption models of three dyes adsorption onto activated carbon prepared waste apricot, Journal of Hazardous Materials 135(1-3) (2006) 232-241.
[100] O. Gercel, A. Ozcan, A.S. Ozcan, H.F. Gercel, Preparation of activated carbon from a renewable bio-plant of Euphorbia rigida by H2SO4 activation and its adsorption behavior in aqueous solutions, Applied Surface Science 253(11) (2007) 4843-4852.
[101] G.G. Stavropoulos, A.A. Zabaniotou, Production and characterization of activated carbons from olive-seed waste residue, Microporous and Mesoporous Materials 82(1-2) (2005) 79-85.
[102] C.X. Yan, C.Q. Wang, J.F. Yao, L.X. Zhang, X.Q. Liu, Adsorption of methylene blue on mesoporous carbons prepared using acid- and alkaline-treated zeolite X as the template, Colloids and Surfaces a-Physicochemical and Engineering Aspects 333(1-3) (2009) 115-119.

[103] H. Tamai, T. Kakii, Y. Hirota, T. Kumamoto, H. Yasuda, Synthesis of extremely large mesoporous activated carbon and its unique adsorption for giant molecules, Chemistry of Materials 8(2) (1996) 454-462.
[104] E.N. El Qada, S.J. Allen, G.M. Walker, Adsorption of basic dyes from aqueous solution onto activated carbons, Chemical Engineering Journal 135(3) (2008) 174-184.
[105] I. Dekany, I. Abraham, L.G. Nagy, K. Laszlo, ENTHALPY OF DISPLACEMENT OF BINARY-LIQUID MIXTURES ON SOLID-SURFACES .3. DETERMINATION OF THE ADSORPTION CAPACITY FROM CALORIMETRIC AND ADSORPTION DATA, Colloids and Surfaces 23(1-2) (1987) 57-68.
[106] X. Liu, D.J. Lee, Thermodynamic parameters for adsorption equilibrium of heavy metals and dyes from wastewaters, Bioresource Technology 160 (2014) 24-31.
[107] I. Anastopoulos, G.Z. Kyzas, Are the thermodynamic parameters correctly estimated in liquid-phase adsorption phenomena?, Journal of Molecular Liquids 218 (2016) 174-185.